frontiers | Frontiers in Microbiology

TYPE Original Research
PUBLISHED 21 April 2023
DOI 10.3389/fmicb.2023.1139633

OPEN ACCESS

EDITED BY
Marianne Quéméneur,
UMR7294 Institut Méditerranéen d'Océanographie (MIO), France

REVIEWED BY
James F. Holden,
University of Massachusetts Amherst, United States
Florence Schubotz,
University of Bremen, Germany

*CORRESPONDENCE
Kaitlin R. Rempfert
✉ kaitlin.rempfert@colorado.edu
Alexis S. Templeton
✉ alexis.templeton@colorado.edu

SPECIALTY SECTION
This article was submitted to Extreme Microbiology, a section of the journal Frontiers in Microbiology

RECEIVED 07 January 2023
ACCEPTED 15 March 2023
PUBLISHED 21 April 2023

CITATION
Rempfert KR, Nothaft DB, Kraus EA, Asamoto CK, Evans RD, Spear JR, Matter JM, Kopf SH and Templeton AS (2023) Subsurface biogeochemical cycling of nitrogen in the actively serpentinizing Samail Ophiolite, Oman. *Front. Microbiol.* 14:1139633. doi: 10.3389/fmicb.2023.1139633

Subsurface biogeochemical cycling of nitrogen in the actively serpentinizing Samail Ophiolite, Oman

Kaitlin R. Rempfert[1]*, Daniel B. Nothaft[1], Emily A. Kraus[2], Ciara K. Asamoto[1], R. Dave Evans[3], John R. Spear[2,4], Juerg M. Matter[5], Sebastian H. Kopf[1] and Alexis S. Templeton[1]*

[1]Department of Geological Sciences, University of Colorado, Boulder, CO, United States, [2]Department of Civil and Environmental Engineering, Colorado School of Mines, Golden, CO, United States, [3]School of Biological Sciences, Washington State University, Pullman, WA, United States, [4]Quantitative Biosciences and Engineering, Colorado School of Mines, Golden, CO, United States, [5]National Oceanography Centre, University of Southampton, Southampton, United Kingdom

Nitrogen (N) is an essential element for life. N compounds such as ammonium (NH_4^+) may act as electron donors, while nitrate (NO_3^-) and nitrite (NO_2^-) may serve as electron acceptors to support energy metabolism. However, little is known regarding the availability and forms of N in subsurface ecosystems, particularly in serpentinite-hosted settings where hydrogen (H_2) generated through water–rock reactions promotes habitable conditions for microbial life. Here, we analyzed N and oxygen (O) isotope composition to investigate the source, abundance, and cycling of N species within the Samail Ophiolite of Oman. The dominant dissolved N species was dependent on the fluid type, with Mg^{2+}-HCO_3^- type fluids comprised mostly of NO_3^-, and Ca^{2+}-OH^- fluids comprised primarily of ammonia (NH_3). We infer that fixed N is introduced to the serpentinite aquifer as NO_3^-. High concentrations of NO_3^- (>100 μM) with a relict meteoric oxygen isotopic composition ($\delta^{18}O \sim 22‰$, $\Delta^{17}O \sim 6‰$) were observed in shallow aquifer fluids, indicative of NO_3^- sourced from atmospheric deposition (rainwater NO_3^-: $\delta^{18}O$ of 53.7‰, $\Delta^{17}O$ of 16.8‰) mixed with NO_3^- produced *in situ* through nitrification (estimated endmember $\delta^{18}O$ and $\Delta^{17}O$ of ~0‰). Conversely, highly reacted hyperalkaline fluids had high concentrations of NH_3 (>100 μM) with little NO_3^- detectable. We interpret that NH_3 in hyperalkaline fluids is a product of NO_3^- reduction. The proportionality of the O and N isotope fractionation ($^{18}\varepsilon$ / $^{15}\varepsilon$) measured in Samail Ophiolite NO_3^- was close to unity ($^{18}\varepsilon$ / $^{15}\varepsilon \sim 1$), which is consistent with dissimilatory NO_3^- reduction with a membrane-bound reductase (NarG); however, abiotic reduction processes may also be occurring. The presence of genes commonly involved in N reduction processes (*narG*, *napA*, *nrfA*) in the metagenomes of biomass sourced from aquifer fluids supports potential biological involvement in the consumption of NO_3^-. Production of NH_4^+ as the end-product of NO_3^- reduction *via* dissimilatory nitrate reduction to ammonium (DNRA) could retain N in the subsurface and fuel nitrification in the oxygenated near surface. Elevated bioavailable N in all sampled fluids indicates that N is not likely limiting as a nutrient in serpentinites of the Samail Ophiolite.

KEYWORDS

serpentinization, water–rock interaction, deep subsurface biosphere, nitrate, nitrogen isotopes, nitrogen, Samail Ophiolite

1. Introduction

The terrestrial subsurface is known to host a substantial biosphere ($2–6 \times 10^{29}$ cells; 23–31 Pg carbon) of diverse microbial communities that likely play significant roles in biogeochemical cycling on a global scale (Nyyssönen et al., 2014; Magnabosco et al., 2018; Flemming and Wuertz, 2019). However, life in the continental subsurface is not uniformly distributed due to heterogeneity in energy availability resulting from differences in host rock lithology and the degree of hydrologic connectivity in the subsurface (Templeton and Caro, in press). Organic matter is scarce in hard-rock subsurface ecosystems, and thus, electron donors derived from minerals are the primary substrate for biological metabolism. Minerals can be directly dissolved by microorganisms, or energy can be released through abiotic chemical reactions (Escudero et al., 2018). For example, hydration and oxidation reactions that occur during the serpentinization of olivine and pyroxene in ultramafic rock can yield reducing power in the form of hydrogen gas (H_2) (McCollom and Bach, 2009). Thus, H_2 generation by serpentinization could fuel microbial life in peridotite rock, where sufficient oxidants are delivered hydrologically. Multiple studies have investigated the diversity and activity of microbial communities likely sustained by H_2 production in serpentinite aquifers (Rempfert et al., 2017; Fones et al., 2019; Sabuda et al., 2020; Seyler et al., 2020; Kraus et al., 2021; Nothaft et al., 2021; Templeton et al., 2021). However, the origins of nutrients and oxidants for these communities have not been sufficiently investigated, and so the broader habitability of subsurface serpentinizing environments remains unconstrained. In particular, the source and principal form of nitrogen (N) in terrestrial serpentinite-hosted ecosystems is unknown.

Nitrogen is essential to all life on Earth as it is required to synthesize proteins, nucleic acids, and many biological macromolecules. Accordingly, the availability of N may control the productivity of ecosystems or the structure of microbial communities where it is limiting. N exists in multiple oxidation states and thus can be utilized by life for energy metabolism in addition to biosynthesis. Reduced nitrogen species such as ammonia/ammonium (NH_3/NH_4^+) may act as electron donors, while N-oxides such as nitrate (NO_3^-) and nitrite (NO_2^-) can serve as electron acceptors. N-oxides are especially important in the deep biosphere because oxidants are often scarce (Jones et al., 2018; Meyer-Dombard and Malas, 2022; Mosley et al., 2022). Determining the source and speciation of N accessible to serpentinite-hosted subsurface life is crucial for understanding how N availability may influence the microbial habitability of subsurface environments. In particular, tracing the fate of NO_3^- could provide insight into the habitability of subsurface rock-hosted environments on other planetary bodies where NO_3^- is likely present, such as Mars (Stern et al., 2017).

We measured the N and oxygen (O) isotopic composition ($\delta^{15}N$ and $\delta^{18}O$, respectively) of dissolved NO_3^- and the N isotopic composition of NH_3/NH_4^+ to assess the origin and transformation of N in the subsurface of a terrestrial serpentinizing system in the Samail Ophiolite, Sultanate of Oman, the world's largest massif of serpentinized peridotite rock (Nicolas et al., 2000). Groundwater fluids were collected from deep boreholes hosted within peridotite and gabbro. The reaction histories of sampled fluids were inferred by geochemical composition, and the speciation and isotopic composition of fluid N were analyzed with the goals of: (1) identifying the major sources of N in the aquifer and (2) evaluating the subsequent biogeochemical cycling of N in the subsurface. In addition, we evaluated possible geologic sources of N by measuring the $\delta^{15}N$ of peridotite rock obtained from diamond drilling during Phase 2 of the Oman Drilling Project (Kelemen et al., 2020). Finally, the potential for microbial participation in the cycling of N at depth was assessed based on the presence of functional genes for N metabolisms in metagenomes derived from biomass collected from borehole fluids. This combined isotopic and functional gene approach yields new insights into the N dynamics of subsurface, serpentinite-hosted ecosystems, revealing how NO_3^- introduced into serpentinite aquifers is primarily converted to NH_4^+, and how NH_3/NH_4^+ is recycled, retaining a substantial pool of fixed N in this subsurface habitat.

2. Methods

2.1. Sampling and geochemical characterization of fluids

We obtained subsurface fluids over four annual field seasons (2015–2018) from 12 boreholes previously drilled by the Oman Ministry of Regional Municipalities and Water Resources. These boreholes are situated in crustal gabbros and mantle peridotites in the Wadi Tayin block of the Samail Ophiolite. We additionally sampled borehole BA1A of the Oman Drilling Project multi-borehole observatory during the 2018 field season; the hydrological properties of this borehole are described extensively in Lods et al. (2020). The lithologies, geographic coordinates, elevations, depths, and casing properties of the boreholes are listed in Table 1.

Detailed descriptions of fluid sampling and aqueous geochemical analyses are reported in Rempfert et al. (2017), Kraus et al. (2021), and Nothaft et al. (2021) for the 2015–2016, 2017, and 2018 field seasons, respectively, with key geochemical parameters summarized in Supplementary Table 1. Briefly, a Grundfos SQ-85 submersible pump was used to collect subsurface fluids for isotopic and metagenomic analyses. Water temperature, pH, and oxidation-reduction potential were measured in the field with a Hach (Loveland, CO) HQ40D Portable Multi Meter. Boreholes were pumped ~20 min prior to sampling until pH stabilized. Biomass was concentrated for DNA extraction on a 0.2-μm Millipore polycarbonate filter. Two aliquots of fluid for isotopic analyses were filtered through a 0.2-μm filter to remove cells and collected in acid-washed 15-ml Falcon tubes (Corning Inc., Corning, NY) (Granger and Sigman, 2009). One aliquot was acidified to a pH of <2 with concentrated hydrochloric acid for the analysis of $\delta^{15}N$ of reduced N (N_{red}) (U. S. Environmental Protection Agency, 1983); the other aliquot was left unacidified for $\delta^{15}N$ and $\delta^{18}O$ analyses of NO_3^- and NO_2^-. Filters for DNA extraction were flash-frozen, transferred in a liquid nitrogen dewar, and stored at −80°C until extraction. Fluid aliquots for isotopic analyses were stored in a cooler on ice in the field, transported *via* air cargo at room temperature, and then stored frozen at −20°C until analysis (Avanzino and Kennedy, 1993; Menchyk et al., 2014).

TABLE 1 Lithology, geographic location, elevation, depth, and borehole properties of wells sampled as previously reported by Rempfert et al. (2017) and Nothaft et al. (2021).

Well	Well depth (mbgl)	Casing extent (mbct)	Screened Interval (mbct)	Depth to water (mbct)	UTM Easting	UTM Northing	Elevation (mabsl)	Lithology
BA1A	400.0	22.0	Open below casing	13.47	674492	2531354	583	peridotite
CM2A	400.0	23.7	Open below casing	13.4	636988	2534284	713	gabbro
NSHQ04	304.0	5.8	Open below casing	4.7	670971	2531699	543	peridotite
NSHQ14	304.0	5.8	Open below casing	9.2	675495	2529716	526	peridotite
WAB103	101.0	101.0	90–98	15	648577	2530362	632	gabbro
WAB104	120.4	120.4	101–104	40	643099	2541124	842	peridotite
WAB105	120.5	120.5	110–117	16.5	644678	2536524	738	peridotite
WAB188	78.0	78.0	35–51	9.5	671123	2529798	514	gabbro
WAB55	102.0	102.0	8–97	7.5	634777	2506101	531	peridotite
WAB71	136.5	136.5	128–131	8.3	670322	2533981	608	peridotite
NSHQ3B	472.0	185.0	91–180	-	645068	2536069	688	alluvium
NSHQ10	304.0	5.8	Open below casing	14.3	645706	2502793	453	peridotite
NSHQ21	233.0	5.4	Open below casing	3.33	633569	2509105	514	gabbro

At BA1A, a packer system (Solexperts) was deployed to sample discrete depth intervals in the borehole. A detailed description of sampling with the packer system is provided by Nothaft et al. (2021).

A single rain event was sampled in 2017 for ~1 min of rainfall by holding an open, acid-washed 15-mL Falcon tube at ~5 ft over the ground. The tube was not opened until after the rain event had started in order to minimize the potential contamination of the sample with dust. The sample was immediately filtered through a 0.2-μm polycarbonate filter to remove cells and prevent the biological processing of N and then placed on ice in a cooler in the field. The sample was stored frozen at −20 °C until the analysis of $\delta^{15}N$ and $\delta^{17}O + \delta^{18}O$ of NO_3^-. Since the sample volume was limited, no second aliquot was acidified for the measurement of reduced N compounds. Because precipitation in Oman is scarce and sporadic (Weyhenmeyer et al., 2002), this sample was the only rainwater obtained during field sampling throughout the multiyear campaign.

2.2. Classification of fluid reaction histories

Serpentinized fluids were categorized as Mg^{2+}-HCO_3^- or Ca^{2+}-OH^- type compositions according to pH and concentrations of $\sum$Mg, $\sum$Ca, and $\sum CO_2$ (Supplementary Table 1) that reflect the extent of water–rock reaction (Barnes et al., 1967; Barnes and O'neil, 1969; Bruni et al., 2002; Paukert et al., 2012; Chavagnac et al., 2013). We infer that Mg^{2+}-HCO_3^- fluids reacted in an open system with atmospheric CO_2 over relatively short residence times, whereas Ca^{2+}-OH^- fluids reacted extensively over long residence times at depths closed to atmospheric inputs (Paukert et al., 2012; Paukert Vankeuren et al., 2019; Leong and Shock, 2020; Leong et al., 2021). The degree of mixing between Mg^{2+}-HCO_3^- and Ca^{2+}-OH^- fluid types was estimated using $\sum$Si as a conservative tracer because $\sum$Si is far more sensitive to mixing than pH in ophiolitic groundwater (Leong et al., 2021). Using the mixing model predictions published by Leong et al. (2021) for endmember Ca^{2+}-OH^- fluids containing 20 μmole/kg $\sum CO_2$, the modeled concentration of $\sum CO_2$ that most closely resembles $\sum CO_2$ measured in highly reacted fluids in this study (Supplementary Table 1), we applied a linear model of $\sum$Si and extent of mixing (%) to our measured fluid compositions (Supplementary Table 2).

2.3. Analysis of aqueous N species

NO_3^- and NO_2^- concentrations were quantified using a Griess reaction-VCl_3 sequential colorimetric assay (García-Robledo et al., 2014) on a BioTek Synergy 2 Microplate Reader. $\sum NH_3$ ($NH_3 + NH_4^+$) concentrations were also quantified spectrophotometrically on a microplate reader using a salicylate hypochlorite colorimetric assay (Ruppersberg et al., 2017).

The $\delta^{15}N$ and $\delta^{18}O$ of NO_3^- and NO_2^- as well as the ^{15}N composition of $\sum NH_3$ were determined using the denitrifier method (Sigman et al., 2001; Weigand et al., 2016) in the Sigman Lab at Princeton University using 20 nmol NO_3^- per analysis. Samples that exhibited >1% NO_2^- were subjected to NO_2^- removal through the sulfamic acid method prior to the analysis of the remaining NO_3^- (Granger and Sigman, 2009) and analyzed in parallel with untreated aliquots ($NO_3^- + NO_2^-$) to allow for the inference of NO_2^- isotopic composition by mass balance. Calibration of isotopic measurements was conducted with the IAEA-NO3 [$\delta^{15}N = 4.7‰$ vs. air, $\delta^{18}O = 25.6‰$ vs. Vienna Standard Mean Ocean Water (VSMOW)] and USGS34 ($\delta^{15}N = -1.8‰$ vs. air, $\delta^{18}O = -27.9‰$ vs. VSMOW) potassium nitrate standards at two concentrations (to correct for volumetric effects) every eight samples with analytical precision: 0.1‰ for $\delta^{15}N$ and

0.3‰ for $\delta^{18}O$ (1σ, $n = 122$). Prior to analysis with the denitrifier method, $\sum NH_3$ was oxidized to NO_3^- *via* the persulfate method using N-clean recrystallized potassium persulfate (Wang et al., 2015). These measurements are reported as $\delta^{15}N$ of N_{red} because persulfate oxidizes all reduced N in the sample. An additional suite of amino acid isotope standards was used to correct for NO_3^- contamination of persulfate (USGS 40, $\delta^{15}N = -4.5‰$; and USGS 41, $\delta^{15}N = 47.6‰$).

The $\delta^{17}O$ measurements of NO_3^- were conducted at the Stable Isotope Core Laboratory at Washington State University using the denitrifier method followed by thermal decomposition of nitrous oxide (N_2O) (Kaiser et al., 2007; Komatsu et al., 2008) with analytical precision 0.84‰ for $\delta^{18}O$ and 0.64‰ for $\delta^{17}O$ (1σ, n =5) using the USGS34 and USGS35 ($\delta^{17}O = 51.50‰$ vs. VSMOW, $\delta^{18}O = 56.81‰$ vs. VSMOW) standards.

Isotopic data are reported with conventional delta notation vs. the international reference scales (air for N; VSMOW for O) in per mil (‰):

$$\delta^{15}N = ([^{15}N/^{14}N]_{sample}/[^{15}N/^{14}N]_{air} - 1)^* 1000 \quad (1)$$

$$\delta^{18}O = ([^{18}O/^{16}O]_{sample}/[^{18}O/^{16}O]_{VSMOW} - 1)^* 1000 \quad (2)$$

$$\delta^{17}O = ([^{17}O/^{16}O]_{sample}/[^{17}O/^{16}O]_{VSMOW} - 1)^* 1000 \quad (3)$$

2.4. Analysis of gaseous N species

The concentration of N_2O was determined from gas sampled by a modified bubble strip method (protocol available at: http://dx.doi.org/10.17504/protocols.io.2x5gfq6). The N_2O was measured with an HNU GC 301 gas chromatograph that was equipped with a Porapak N column under P-5 carrier gas (95% argon, 5% methane) at the USGS Water Mission Area Laboratories in Boulder as described in Repert et al. (2014) with a coefficient of variation for triplicate measurements of 11%.

2.5. Analysis of rock-N

Three peridotite rock core samples from the 280-meter depth interval in boreholes BA3A, BA4A, and BA1B of the multi-borehole observatory were obtained during Phase 2 of the Oman Drilling Project. Sampling procedures for clean retrieval of rock core are detailed in Templeton et al. (2021). Bulk $\delta^{15}N$ of powdered peridotite was measured *via* continuous-flow isotope ratio mass spectrometry using the sealed tube combustion method (Boocock et al., 2020) on a Thermo Finnigan MAT253 in the St Andrews Stable Isotope Geochemistry (STAiG) laboratory. All three samples exhibited a signal/blank ratio >10:1.

2.6. N-cycling functional gene analysis

Metagenomic data for this study were previously published by Fones et al. (2019) and Kraus et al. (2021), including procedures regarding DNA extraction, metagenomic library prep, and sequencing. In short, DNA extraction was conducted according to the manufacturer's instructions with a MoBio PowerSoil Kit or Zymo Research Xpedition Soil/Fecal DNA MiniPrep extraction kit for samples collected in 2015 and 2017, respectively. Triplicate extractions were pooled, quantified, and normalized to 1 ng before library preparation using the Nextera XT kit. After tagmentation and amplification, products were pooled equimolarly and sequenced on an Illumina MiSeq platform (2x150 bp) at the University of Colorado Next-Generation Sequencing Facility (2015 samples) or an Illumina HiSeq 2,500 platform (2 x 250 bp) at the Duke Center for Genomic and Computational Biology (2017 samples).

Demultiplexed metagenomic sequences were merged (minimum length of 30), low-quality bases were trimmed off read ends (<15), and reads of <100 bases were discarded using the AdapterRemoval v2 (Schubert et al., 2016). Reads were quality filtered and then aligned to the NCycDB database (95% clustering) (Tu et al., 2019) for the identification of N-cycling genes using the Diamond aligner (Buchfink et al., 2015). Gene homolog abundances were normalized to metagenome size, and results from the two sampling years were combined.

2.7. Calculations of ^{17}O difference ($\Delta^{17}O$)

The $\Delta^{17}O$ can be determined by the following equation provided by Miller (2002):

$$\Delta^{17}O = \left[\ln\left(1 + \frac{\delta^{17}O}{1000}\right) - 0.52 \cdot ln\left(1 + \frac{\delta^{18}O}{1000}\right) \cdot 1000\right] \quad (4)$$

The fraction of atmospheric endmember NO_3^- (f_{atm}) in an aquifer fluid can be calculated through a simple mass balance:

$$\Delta^{17}O_{mixed} = f_{biogeo}(\Delta^{17}O_{biogeo}) + f_{atm}(\Delta^{17}O_{atm}) \quad (5)$$

where $\Delta^{17}O_{mixed}$ is the ^{17}O difference of NO_3^- in a mixed aquifer fluid presumed to represent some fraction of atmospheric endmember NO_3^- ($\Delta^{17}O_{atm}$) and biogeochemical endmember NO_3^- ($\Delta^{17}O_{biogeo}$) ^{17}O. The $\Delta^{17}O_{biogeo}$ can be assumed to equal 0 because biogeochemical processes follow mass-dependent fractionation. Accordingly, equation (5) simplifies to:

$$f_{atm} = \Delta^{17}O_{mixed}/(\Delta^{17}O_{atm}) \quad (6)$$

For $\Delta^{17}O_{atm}$, we used the measured $\Delta^{17}O$ of sampled rainwater. We recognize a single rainwater sample may not be entirely representative of the isotopic composition of mean annual rainfall since the $\Delta^{17}O$ of dissolved NO_x in rainwater has been documented to fluctuate ~15‰ seasonally (Saud et al., 2022). The measured $\Delta^{17}O$ is in the lower range expected for atmospheric deposition (Savard et al., 2018), with $\Delta^{17}O$ values for atmospheric NO_x typically ranging between ~ 20–32‰ (Michalski et al., 2003). Accordingly, we applied an uncertainty of +15‰ for this endmember composition in mass balance calculations, using a $\Delta^{17}O_{atm}$ of 31.8‰ to conservatively estimate f_{atm}.

3. Results

3.1. Geochemical context of ophiolite fluids

Mg^{2+}-HCO_3^- fluids were characterized by alkaline pH (8.3–9.2) and relatively high ∑Mg and ∑CO_2 concentrations (0.37–3.3 mM and 1.3–3.6 mM, respectively) compared to the hyperalkaline pH (10–11.4) and high ∑Ca concentrations (0.43–7.8 mM) of Ca^{2+}-OH^- fluids (Supplementary Table 1). The Ca^{2+}-OH^- fluids also typically contained μM to mM concentrations of dissolved H_2 and CH_4. Of the wells sampled in this study, six wells hosted in peridotite were classified as Mg^{2+}-HCO_3^- type fluids, representing open-system water–rock reaction under relatively oxidized conditions (Eh 78 to 180 mV), and seven wells as Ca^{2+}-OH^- type fluids, representing closed-system water–rock reaction under highly reducing conditions (Eh as low as−415 mV).

To assess the degree of mixing of deep, reacted Ca^{2+}-OH^- fluids with less reacted Mg^{2+}-HCO_3^- fluids in the near surface, we applied the Leong et al. (2021) approach of using ∑Si as a conservative tracer for the mixing of reacted fluids in ophiolitic aquifers. The composition of fluids collected in this study is plotted along the Leong et al. (2021) reaction path model (Figure 1) for the progressive reaction of rainwater with peridotite during serpentinization. No Ca^{2+}-OH^- fluids sampled in this study displayed ∑Si concentrations as low as expected for chrysotile-brucite-calcite±diopside equilibrium, indicating some degree of mixing with Mg^{2+}-HCO_3^- fluids. From our calculations of endmember fluid mixing (Supplementary Table 2), most Ca^{2+}-OH^- fluids were mixed with <10% Mg^{2+}-HCO_3^- type fluids, except fluids sampled from BA1A from the 100–400 m packed interval and from well WAB56 which indicated mixing of ∼15% and 57–73% Mg^{2+}-HCO_3^- fluids, respectively. Fluids hosted within gabbro plotted with Mg^{2+}-HCO_3^- fluids, but with slightly higher ∑Si concentrations.

3.2. Concentration and isotopic composition of dissolved N species

The predominant dissolved N species was dependent on the fluid type, with alkaline Mg^{2+}-HCO_3^- type peridotite-hosted fluids and fluids hosted in gabbro comprised mostly of NO_3^-, and hyperalkaline Ca^{2+}-OH^- peridotite-hosted fluids comprised primarily of reduced N (∑NH_3) (Figure 2). The Mg^{2+}-HCO_3^- type fluids contained NO_3^- concentrations between 66 and 146 μM, while Ca^{2+}-OH^- fluids only contained up to 26 μM (Table 2). Conversely, Ca^{2+}-OH^- fluids were enriched in NH_3 (up to 114 μM), while ∑NH_3 concentrations were ∼5 μM in all Mg^{2+}-HCO_3^- type fluids (Table 3).

Fluids hosted within gabbros were also dominated by NO_3^-, but with higher concentrations (as high as 366 μM) than observed for Mg^{2+}-HCO_3^- fluids. Both Mg^{2+}-HCO_3^- and Ca^{2+}-OH^- type fluids had lower concentrations of NO_3^- than observed in rainwater (252 μM); however, gabbro well WAB103 demonstrated concentrations of NO_3^- greater than rainwater. NO_2^- was often detectable across fluid types, but in very low concentrations (∼1 μM) except for in a few fluids where NO_2^- was present at concentrations between ∼4 and 30 μM (Table 4). All wells where dissolved N_2O concentrations were analyzed contained detectable

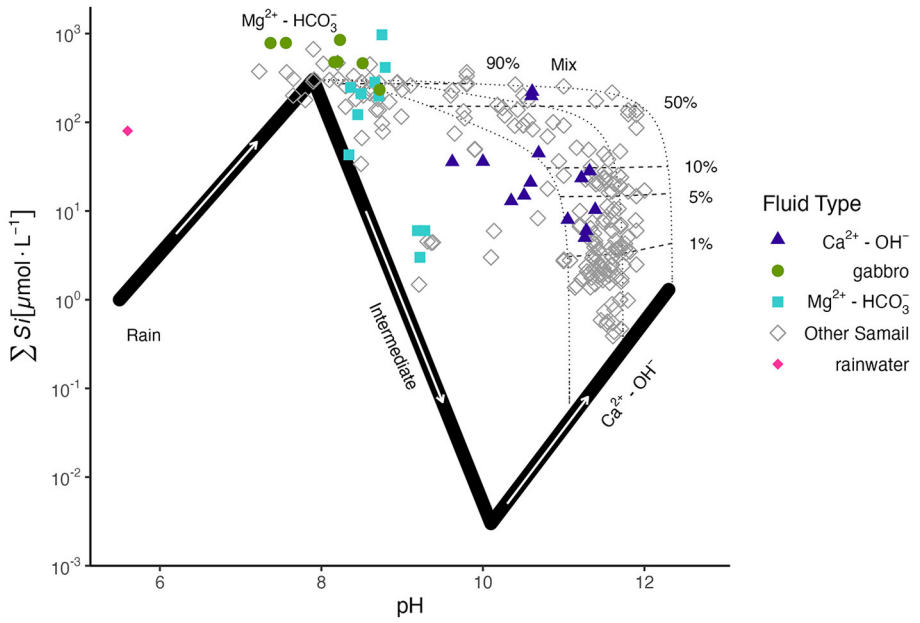

FIGURE 1
∑Si vs. pH of sampled fluids in this study, colored by fluid type, and of other Samail Ophiolite data (Stanger, 1986; Dewandel et al., 2004; Chavagnac et al., 2013; Rempfert et al., 2017; Leong et al., 2021) in gray, with the reaction path model of Leong et al. (2021) for the progressive reaction of rainwater with peridotite rock. Three potential Ca^{2+}-OH^- compositions of varying ∑CO_2 (8, 10, 20 μmole/kg from right to left) are plotted. ∑Si is used as a conservative tracer to distinguish the extent of mixing between Ca^{2+}-OH^- and Mg^{2+}-HCO_3^- fluids (shown in the plot as percentages next to mixing tie-lines). Mixing proportions are reported in Supplementary Table 2.

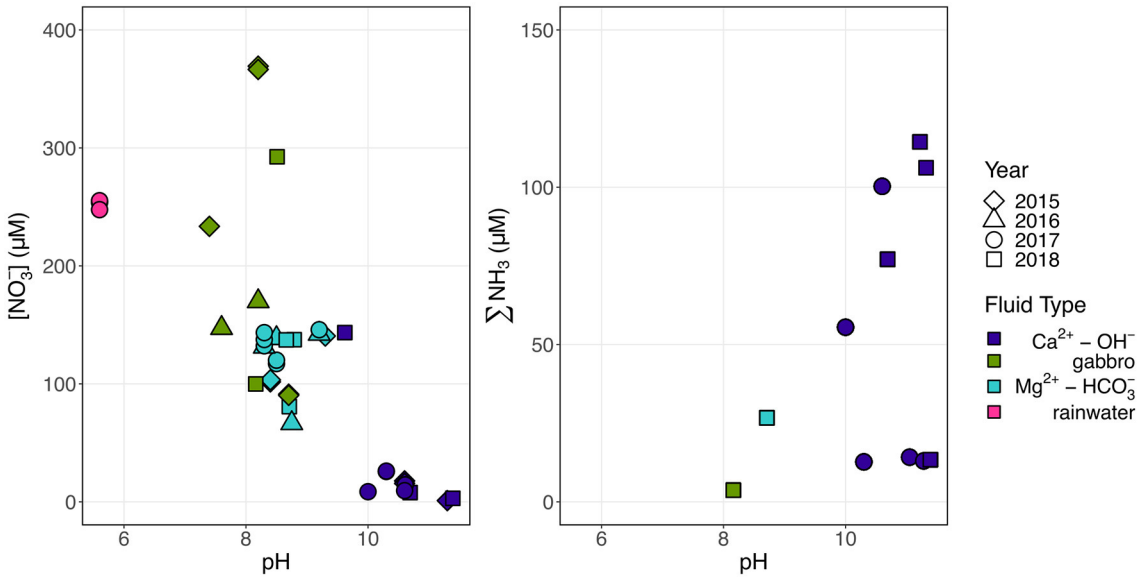

FIGURE 2
Trend of decreasing NO_3^- concentrations and increasing $\sum NH_3$ concentrations with pH. Colors indicate fluid composition and shapes indicate the year of sampling.

N_2O, which varied in concentration from 5 to 177 nM, with the highest concentration observed in the packed-off interval 55–66 m in borehole BA1A (Table 5).

The dual isotopic composition of NO_3^- ($\delta^{15}N$ and $\delta^{18}O$) offers valuable information on potential sources and subsequent transformations of NO_3^- in the subsurface, aquifer ecosystem. On a biplot of $\delta^{15}N$ and $\delta^{18}O$ of NO_3^- (Figure 3), Oman rainwater plots within the range expected for atmospheric deposition (Oman rainwater: $\delta^{15}N$ −2.2‰, $\delta^{18}O$ 55.6‰) (Kendall Carol, 1998; Kendall et al., 2007). A few Ca^{2+}-OH^- fluids, where NO_3^- concentrations are <26 μM, plot within the range expected for nitrification-derived NO_3^- ($\delta^{18}O$ < 10‰) (Kendall Carol, 1998; Kendall et al., 2007). However, most Samail ophiolite aquifer fluids exhibit $\delta^{18}O$ between these two sources, indicating the likely contribution of NO_3^- from both atmospheric and biological nitrification sources.

To investigate atmospheric deposition as a potential source of NO_3^- to the aquifer, we measured the $\delta^{17}O$ of oxidized aqueous N species ($NO_x = NO_2^- + NO_3^-$) in a subset of samples from the 2017 and 2018 field seasons. Atmospherically sourced NO_3^- and NO_2^- have $\delta^{17}O$ higher than predicted for mass-dependent fractionation due to photochemical reactions with ozone in the stratosphere (Thiemens, 1999, 2006; Lyons, 2001; Mauersberger et al., 2001; Michalski et al., 2002, 2003, 2004). Because subsequent biological fractionation of atmospherically derived NO_3^- should not impact the deviation of $\delta^{17}O$ in oxidized N species from expected mass-dependent fractionation ($\Delta^{17}O$ of NO_x), the $\Delta^{17}O$ of measured NO_x can be used to calculate the relative contribution of biogeochemical and atmospheric sources of NO_3^- (Michalski et al., 2003; Riha et al., 2014). Biogeochemical sources, such as nitrification-derived NO_3^-, are assumed to have a mass-dependent $\Delta^{17}O$ value of 0‰. We found that all measured fluids contained NO_3^- which reflected some contribution of a relict atmospheric source, with $\Delta^{17}O$ above 0‰ (Table 6). The $\Delta^{17}O$ was highest in Mg^{2+}-HCO_3^- type peridotite-hosted fluids (Figure 4) and generally correlated with the $\delta^{18}O$ and concentration of NO_3^-. These $\Delta^{17}O$ corresponded to estimated fractions of atmospheric endmember NO_3^- (f_{atm}) ranging from 0.09 to 0.41, accounting for uncertainty in the endmember $\Delta^{17}O_{atm}$ isotopic composition.

By mass balance, the isotopic composition of biogeochemically derived NO_3^-, $\delta^{18}O$ NO_3^- $_{biogeo}$, can be calculated (Supplementary Table 3). The $\delta^{18}O$ NO_3^- $_{biogeo}$ reflects NO_3^- produced by nitrification as well as processes that act to enrich the NO_3^- pool, such as nitrate reduction (NR) during biological assimilation or respiration. Most measured samples exhibited $\delta^{18}O$ NO_3^- $_{biogeo}$ <10‰, consistent with nitrification-derived NO_3^- (Kendall et al., 2007; Xue et al., 2009; Kaushal et al., 2011; Yi et al., 2017). However, fluids collected from borehole BA1A with the packer system to isolate deep Ca^{2+}-OH fluids below 100 m had $\delta^{18}O$ of 27‰, suggesting extensive NR. Biological NR causes the $\delta^{18}O$ and $\delta^{15}N$ of NO_3^- in the residual pool to increase in a relatively predictive pattern, with the proportionality of N and O isotopic fractionation varying between 0.5 and 1 (Böttcher et al., 1990; Sigman et al., 2005; Granger et al., 2008; Chen and MacQuarrie, 2011; Knöller et al., 2011; Granger and Wankel, 2016; Asamoto et al., 2021). We observed a general trend of coupled increase in $\delta^{18}O$ and $\delta^{15}N$ of NO_3^- with a proportionality of ~1 (Figure 3), consistent with NR.

The $\delta^{15}N$ of reduced nitrogen species (N_{red}) spanned a range of 30‰ (Table 4). In most samples, $\sum NH_3$ concentrations were comparable to the concentration of N_{red} measured *via* the mass balance of total N after persulfate oxidation compared to total oxidized nitrogen species ($NO_x = NO_3^- + NO_2^-$); however, this was not true in samples from WAB188 and NSHQ14 where concentrations of N_{red} were greater than

TABLE 2 $\delta^{15}N$ and $\delta^{18}O$ of NO_3^- with NO_3^- concentration measured by the denitrifier method.

Sample	Year	Fluid type	NO_3^- [μM]	$\delta^{15}N$ NO_3^- ‰	$\delta^{18}O$ NO_3^- ‰
BA1A_100_400m	2018	Ca^{2+}-OH^-	7.8 ± 0.1	25.2 ± 0.09	34.6 ± 0.5
BA1A_55_66m	2018	Mg^{2+}-HCO_3^-	80.7 ± 3.2	6.1 ± 0.06	26.8 ± 0.3
NSHQ10	2016	Mg^{2+}-HCO_3^-	66.6 ± 1.1	20.1 ± 0.05	24.3 ± 0.3
NSHQ14	2015	Ca^{2+}-OH^-	1 ± 0.1	15.9 ± 0.09	20.6 ± 0.7
NSHQ14	2018	Ca^{2+}-OH^-	3 ± 0.1	5.6 ± 0.06	12.7 ± 0.5
NSHQ14_18m	2017	Ca^{2+}-OH^-	25.8 ± 1.4	10.6 ± 0.24	9.5 ± 0.3
NSHQ21	2015	Gabbro	233 ± 2.5	9.0 ± 0.07	14.9 ± 0.2
NSHQ3B	2015	Mg^{2+}-HCO_3^-	102.5 ± 1.1	2.8 ± 0.05	21.7 ± 0.2
NSHQ4	2017	Ca^{2+}-OH^-	8.6 ± 0.5	4.0 ± 0.2	19.5 ± 0.3
rainwater	2017	rainwater	252.2 ± 9.0	−2.2 ± 0.2	55.6 ± 0.3
WAB103	2015	Gabbro	367.9 ± 4	8.9 ± 0.06	16.7 ± 0.2
WAB103	2016	Gabbro	169.9 ± 2.1	11.8 ± 0.04	18.9 ± 0.2
WAB103	2018	Gabbro	292.5 ± 4.9	10.5 ± 0.06	18.1 ± 0.3
WAB104	2016	Mg^{2+}-HCO_3^-	138.6 ± 2	1.4 ± 0.03	22.9 ± 0.2
WAB104	2017	Mg^{2+}-HCO_3^-	118.6 ± 5.9	2.3 ± 0.2	22.9 ± 0.3
WAB104	2018	Mg^{2+}-HCO_3^-	137.5 ± 3.4	1.1 ± 0.06	23.5 ± 0.3
WAB105	2016	Mg^{2+}-HCO_3^-	131.4 ± 1.5	2 ± 0.03	23.6 ± 0.2
WAB105	2017	Mg^{2+}-HCO_3^-	137.8 ± 4.9	2.5 ± 0.1	21.8 ± 0.6
WAB105	2018	Mg^{2+}-HCO_3^-	137.3 ± 3.1	2.2 ± 0.06	22 ± 0.3
WAB188	2015	Gabbro	90.7 ± 1	5.5 ± 0.05	22.5 ± 0.2
WAB188	2016	Gabbro	147.3 ± 1.7	3.3 ± 0.03	21.8 ± 0.2
WAB188	2017	Gabbro	135.9± 6.2	5.5 ± 0.04	22.5 ± 0.2
WAB188	2018	Gabbro	99.9 ± 3.1	3.2 ± 0.06	21.3 ± 0.3
WAB55	2015	Mg^{2+}-HCO_3^-	140 ± 1.5	7.4 ± 0.07	21.1 ± 0.2
WAB55	2016	Mg^{2+}-HCO_3^-	142.3 ± 1.7	7.5 ± 0.03	20.8 ± 0.2
WAB55	2017	Mg^{2+}-HCO_3^-	145.9 ± 0.9	8.8 ± 0.05	20.9 ± 0.2
WAB55	2018	Ca^{2+}-OH^-	143.5 ± 2.9	7.8 ± 0.06	20.5 ± 0.3
WAB56	2015	Ca^{2+}-OH^-	16.7 ± 0.3	20.7 ± 0.09	30.7 ± 0.2
WAB56	2017	Ca^{2+}-OH^-	14.4 ± 0.8	9.94 ± 0.23	22.8 ± 0.3
WAB71	2017	Ca^{2+}-OH^-	9.5 ± 0.5	13.2 ± 0.26	0.9 ± 0.3

Standard error is calculated from all experimental replicates.

measured $\sum NH_3$. In these wells, the $\delta^{15}N$ of N_{red} must be interpreted as a mixture of $\sum NH_3$ and other dissolved forms of reduced N, such as organic compounds. The $\delta^{15}N$ of N_{red} varied considerably, with the highest $\delta^{15}N$ (13.6‰) observed for borehole WAB71 where the concentration of NH_3 was greatest (114 μM).

3.3. Bulk rock N abundance and $\delta^{15}N$

Nitrogen can be stored in rocks as recalcitrant organic matter, NH_4^+ or NO_3^- salts, nitride minerals, substituted in hydrous minerals, incorporated into the structure of silicate minerals, or as gas within fluid inclusions (Holloway and Dahlgren, 2002; Loganathan and Kalinichev, 2013; Mysen, 2019). Because this N could be liberated or assimilated during water–rock reaction (Silver et al., 2012; Houlton et al., 2018), we measured the abundance of bulk N in peridotite rock using the sealed tube combustion method which allows for the measurement of even stably bound N within the silicate mineral structure (Bebout et al., 2007; Boocock et al., 2020). N abundances were low (11.3–13.9 ppm) in analyzed peridotite rock core samples and bulk $\delta^{15}N$ of peridotite samples varied from 3.5 to 6.7‰ (Table 7).

TABLE 3 $\delta^{15}N$ of N_{red} which represents the total reduced nitrogen in the sampled fluid (measured by the denitrifier method through mass balance after persulfate oxidation).

Sample	Fluid type	Year sampled	N_{red} [μM]	$\sum NH_3$ [μM]	$\delta^{15}N_{red}$ ‰
BA1A_100_400m	Ca^{2+}-OH^-	2018	80.2 ± 7.6	77.1 ± 10.0	−12.9 ± 1.5
BA1A_55_66m	Mg^{2+}-HCO_3^-	2018	32.0 ± 12.3	26.7 ± 0.5	−16.7 ± 6.5
CM2A	Ca^{2+}-OH^-	2018	99.1 ± 8.8	106.2 ± 5.9	6.9 ± 0.9
NSHQ14	Ca^{2+}-OH^-	2018	28.3 ± 2.4	13.4 ± 2.4	4.6 ± 0.5
NSHQ14_18m	Ca^{2+}-OH^-	2017	20.4 ± 1.2	12.7 ± 0.4	5.0 ± 0.6
NSHQ14_50m	Ca^{2+}-OH^-	2017	23.0 ± 0.4	14.2 ± 0.3	9.6 ± 0.2
NSHQ14_85m	Ca^{2+}-OH^-	2017	18.1 ± 0.3	13.0 ± 0.3	4.3 ± 0.2
NSHQ4	Ca^{2+}-OH^-	2017	50.7 ± 1.2	55.5 ± 5.0	0.9 ± 0.1
WAB188	Gabbro	2018	41.8 ± 14.5	3.7 ± 1.0	2.4 ± 1.4
WAB56	Ca^{2+}-OH^-	2017	141.6 ± 2.4	-	3.4 ± 0.1
WAB71	Ca^{2+}-OH^-	2017	109.6 ± 2.0	100.3 ± 1.9	11.2 ± 0.3
WAB71	Ca^{2+}-OH^-	2018	105.6 ± 11.1	114.4 ± 3.1	13.6 ± 2.0

Standard error is calculated from all experimental replicates. Concentrations of NH_3 via colorimetric assay are provided for comparison.

TABLE 4 δ15N and δ18O of NO_2^- with NO_2^- concentration measured by mass balance by the denitrifier method after NO_2^- removal with sulfamic acid.

Sample	Year	Fluid type	NO_2^- [μM]	$\delta^{15}N$ NO_2^- ‰	$\delta^{18}O$ NO_2^- ‰
NSHQ10	2016	Gabbro	30.3 ± 1.6	−17.9 ± 1.3	5.2 ± 1.7
NSHQ4	2017	Ca^{2+}-OH^-	4.8 ± 0.8	−4.4 ± 1.0	21.1 ± 3.1
WAB56	2015	Ca^{2+}-OH^-	3.8 ± 0.4	7.8 ± 2.3	22.5 ± 3.3

Errors reported are propagated errors for replicate analyses.

TABLE 5 Concentrations of dissolved N_2O measured in gases collected from the 2018 fluids *via* the bubble strip method.

Sample	Fluid type	$N_2O_{(g)}$ [nM]
BA1A-100-400m	Ca^{2+}-OH^-	5.05E00
BA1A-55-66m	Mg^{2+}-HCO_3^-	1.77E02
CM2A	Ca^{2+}-OH^-	5.13E00
NSHQ14	Ca^{2+}-OH^-	8.70E00
WAB103	gabbro	2.45E01
WAB104	Mg^{2+}-HCO_3^-	2.03E01
WAB105	Mg^{2+}-HCO_3^-	1.67E01
WAB188	gabbro	1.26E01
WAB55	Ca^{2+}-OH^-	1.87E01
WAB71	Ca^{2+}-OH^-	1.47E01

3.4. Presence of N-cycling genes

To assess the possibility of microbial involvement in the cycling of N within Samail Ophiolite aquifers, we used metagenomic sequencing of groundwater fluid biomass to probe for genes known to be involved in N utilization or transformation (Figure 5). N-cycling gene homologs were fairly ubiquitous across sampled fluids, albeit in low abundance (<2 gene homologs/Mb of sequence). Gene homologs associated with NR, both assimilatory *narB* and dissimilatory reductases *narG* and *napA*, were most abundant although homologs for the cytochrome c nitrite reductase (*nrfA*) involved in the reduction of NO_2^- to NH_4^+ in dissimilatory nitrate reduction to ammonium (DNRA) were also notably abundant across fluids. We did not observe any major trends in gene absence or presence by fluid type.

It is important to note that these methods only detect the presence of these genes in aquifer fluids, and do not indicate whether individual organisms possess all genes involved in any specific N-cycling pathway, or whether these genes are actively expressed or utilized. Nevertheless, the presence of gene homologs for N-cycling processes in Samail Ophiolite fluids suggests the potential for biological transformations.

4. Discussion

4.1. Rainwater delivers atmospheric N to Samail Ophiolite aquifers

The positive measured $\Delta^{17}O$ of NO_3^- for all sampled groundwaters suggests atmospheric deposition is a primary source of N to Samail Ophiolite aquifers. The degree to which NO_3^- is sourced from the atmosphere can be estimated using the $\delta^{17}O$ of NO_3^- as a conservative tracer. During ozone formation, the ratio of $^{18}O/^{16}O$ becomes equally elevated as the ratio of $^{17}O/^{16}O$, thus enriching both isotopes independent of their mass difference (Thiemens and Heidenreich, 1983; Thiemens et al., 2001;

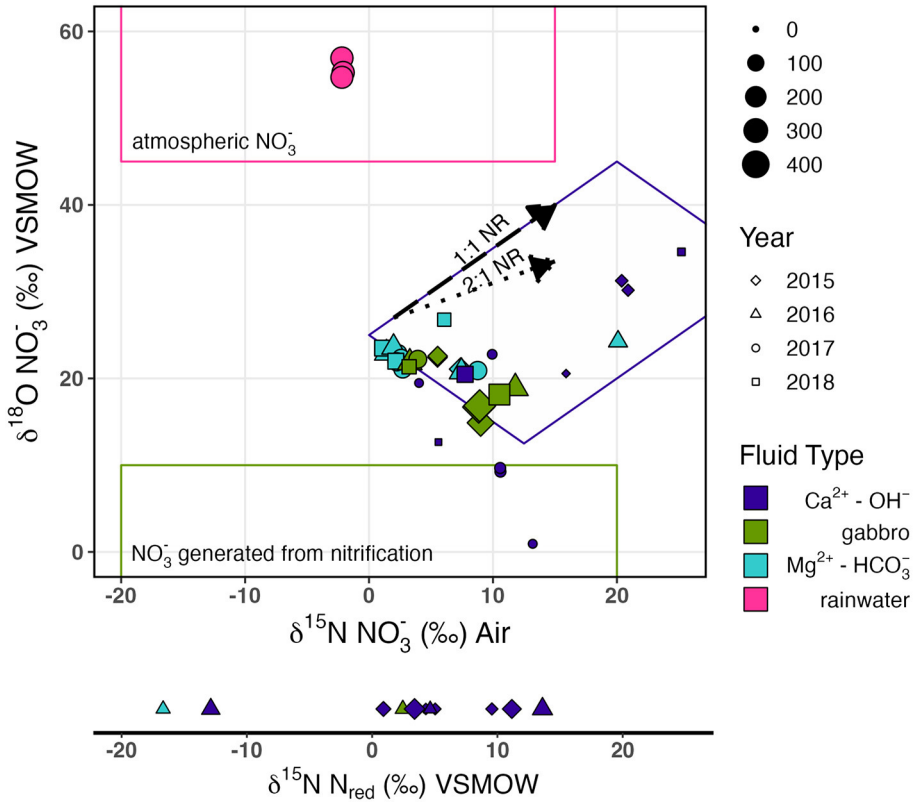

FIGURE 3
$\delta^{18}O$ vs. $\delta^{15}N$ of NO_3^- biplot, with the $\delta^{15}N$ of reduced N plotted on the same scale. Colors indicate fluid type, shapes indicate the year of sampling, and the size of points represents the concentration of N species in μM. Trends for NR with a slope of 1 (labeled 1:1; long dash) and 0.5 (labeled 2:1 with dotted arrow) are illustrated. The field outlined in pink represents the common isotopic composition for atmospheric NO_3^-, the field outlined in green represents the common isotopic composition of nitrified NO_3^-, and the field outlined in purple represents samples with ^{15}N- and ^{18}O-enriched isotopic compositions consistent with NR. Isotopic fields for common isotopic compositions were sourced from Kendall et al. (2007).

TABLE 6 $\delta^{17}O$ and $\delta^{18}O$ isotopic compositions of NO_3^-.

Sample	Year sampled	$\delta^{18}O\ NO_3^-$ (‰)	$\delta^{17}O\ NO_3^-$ (‰)	$\Delta^{17}O\ NO_3^-$ (‰)	f_{atm}
Rainwater	2017	53.7 (1.8)	44.7 (3.6)	16.8 (2.7)	1 [0.47]
WAB104	2018	19.6 (1.0)	17.1 (0.7)	6.9 (1.2)	0.41 [0.19]
BA1A 100-400m packed interval	2018	32.8	21.3	4.3	0.25 [0.12]
BA1A 55-66m packed interval	2018	26.4	20.7	6.9	0.41[0.19]
NSHQ14	2018	19.3	13.1	3.1	0.18 [0.09]
WAB104	2017	23.2	17.7	5.7	0.34 [0.16]
WAB105	2018	22.5	18.4	6.7	0.40 [0.19]
WAB188	2018	22.3	16.1	4.5	0.27 [0.13]
WAB55	2018	20.89	15.0	4.09	0.24 [0.11]

^{17}O difference ($\Delta^{17}O$) and corresponding calculated atmospheric endmember fractional contribution to the observed $\Delta^{17}O$ signatures of NO_3^- in borehole fluids are also reported. Errors (1σ, n = 2) for replicate measures are displayed in parentheses. Conservative estimates of f_{atm}, displayed in brackets, were calculated by applying an uncertainty of 15‰ for expected endmember $\Delta^{17}O_{atm}$ composition.

Miller, 2002). Ozone then transfers O atoms during oxidation reactions that result in a positive $\Delta^{17}O$ of many oxygen sources in the atmosphere (O_3, O_2, H_2O) which can be inherited by N-oxides during photochemical reaction (typically $\Delta^{17}O$ of 20–32‰) (Savarino et al., 2000, 2008; Lyons, 2001; Michalski et al., 2012). Mixing with biogeochemically sourced NO_3^- would lower $\Delta^{17}O$ toward 0‰ (Casciotti et al., 2002; Michalski et al., 2003; Ewing et al., 2007; Kendall et al., 2007; Dejwakh et al., 2012; Riha et al.,

TABLE 7 Bulk rock δ15N of peridotites sampled at the 280-m depth interval in boreholes BA1B, BA3A, and BA4A.

Borehole	Depth [m]	ppm N	$\delta^{15}N$ N_{bulk} ‰
BA1B	280	11.3	4.4
BA3A	280	13.9	3.54
BA4A	280	11.3	6.66

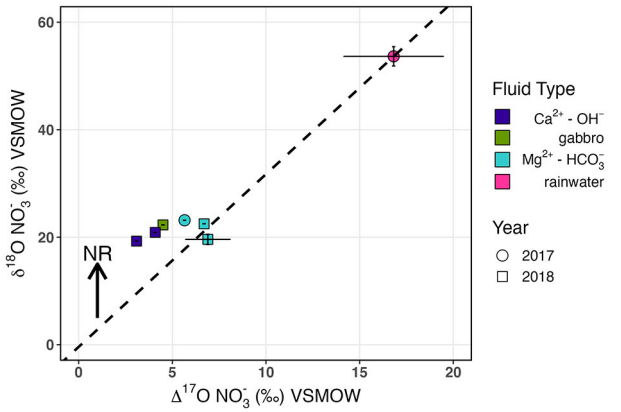

FIGURE 4
$\delta^{18}O$ vs. $\Delta^{17}O$ of NO_3^-. Mg^{2+}-HCO_3^- fluids (blue) plot on a theoretical mixing line with rainwater (pink) calculated for simple mixing of estimated end-member nitrified NO_3^- ($\delta^{18}O$ of−0.4‰ and $\Delta^{17}O$ of 0‰). NO_3^- reduction would lead to increased $\delta^{18}O$ with no change in $\Delta^{17}O$.

2014). We measured a range of $\Delta^{17}O$ for groundwater NO_3^- of 3.1 to 6.9‰, corresponding to estimated atmospheric endmember contributions of 18 to 41% using a simple two-member isotope mixing model (Table 6).

This atmospheric contribution represents both wet and dry deposition. The concentration of NO_3^- in rainwater was high (~255 μM), but precipitation in Oman is scarce and sporadic, with elevations below 1000 m typically receiving only 60–100 mm of rainfall per year from mostly Mediterranean frontal systems (Weyhenmeyer et al., 2002). Accordingly, dry deposition may contribute a more significant flux of N to Samail Ophiolite aquifers compared to wet deposition. While not well constrained, up to 82% of atmospheric NO_x deposition occurs as dry deposition in arid regions of central Asia (Li et al., 2013). An atmospheric origin of NO_3^- is consistent with reports for soil crusts in desert environments such as the Mojave and the Atacama as well as in catchments in the southwestern United States where 31 to 100% of soil nitrate and up to 82% of stream nitrate is atmospherically derived (Böhlke et al., 1997; Michalski et al., 2004; Lybrand et al., 2013; Riha et al., 2014).

A partial atmospheric source for the measured NO_3^- in shallow aquifer fluids would require effective transference of N to the subsurface. Despite low annual rainfall, the effective rainfall in the Samail Ophiolite is relatively high. In a hydrologic study conducted in the Ibra region of the Samail Ophiolite by Dewandel et al. (2005), 50 mm of rain per year was estimated to be effective rain, of which 18 ± 8 mm is presumed to recharge shallow peridotite aquifers. Estimated recharge into gabbro is predicted to be even higher (>20 mm/year) on account of the greater hydraulic conductivity of gabbros compared to peridotites in the Samail Ophiolite (10^{-5} to 10^{-6} for gabbro and 10^{-7} for serpentinized peridotite) and the likely additional input of surface runoff due to the moderate relief of gabbro outcrops, both of which could explain the higher NO_3^- concentrations observed in some gabbro wells (Dewandel et al., 2005). The absence of soil or major vegetation in this environment further facilitates the rapid transfer of rainwater to the subsurface before significant biological processing can remove N from the infiltrating fluids.

4.2. Nitrification-derived NO_3^- comprises the rest of the groundwater NO_3^- Pool

The remaining 59–91% of subsurface NO_3^- can be explained by biological nitrification. Nitrification is one of the two biological processes that produce NO_3^- during the biogeochemical cycling of N (Granger and Wankel, 2016). In this two-step process, NH_3 is oxidized to NO_2^- and then NO_3^-, coupled with aerobic respiration (Verstraete and Focht, 1977; Teske et al., 1994). Both bacteria and archaea mediate NH_3 oxidation, but only bacteria are known to carry out the NO_2^- oxidation step, with some bacterial taxa capable of completely oxidizing NH_3 to NO_3^- (comammox) (Daims et al., 2015; van Kessel et al., 2015). We detected both archaeal and bacterial functional markers for NH_3 oxidation (*amoA* gene), with no differential abundance by fluid type, despite $\sum NH_3$ concentration acting as a strong selector for NH_3 oxidizing taxa in other environments (Martens-Habbena et al., 2009; Bates et al., 2011; Verhamme et al., 2011; Lehtovirta-Morley, 2018). NH_3 oxidation is presumed to be primarily aerobic because we only sparsely detected gene homologs for hydrazine dehydrogenase (*hdh*), which encodes the key enzyme in anaerobic ammonia oxidation (anammox) for catalyzing hydrazine oxidation to N_2 gas (Kartal et al., 2007; Maalcke et al., 2016) (see Supplementary datasheet).

In NH_3 oxidation to NO_2^-, O is incorporated enzymatically from O_2 and H_2O in a 1:1 ratio, whereas in NO_2^- oxidation to NO_3^-, O is solely derived from H_2O (Andersson and Hooper, 1983; Buchwald and Casciotti, 2010). The $\delta^{18}O$ of nitrified NO_3^- has been shown to closely resemble the isotopic composition of ambient H_2O in both labeled nitrifying incubations (Boshers et al., 2019) and field observations (Buchwald and Casciotti, 2010; Buchwald et al., 2012). Accordingly, we presume that nitrified NO_3^- in Samail Ophiolite aquifers should have a $\delta^{18}O$ of−0.4‰, which represents the average $\delta^{18}O$ of aquifer H_2O measured from a subset of 2018 Mg^{2+}-HCO_3^- and Ca^{2+}-OH^- fluids (Supplementary Table 4). Utilizing this estimated value of−0.4‰ for $\delta^{18}O$ of NO_3^- along with a $\Delta^{17}O$ of 0‰ as a nitrification "end-member" for Samail Ophiolite fluids, we applied a simple two-member isotope mixing model with NO_3^- in rainwater (NO_3^- $\delta^{18}O$ 53.7‰, $\Delta^{17}O$ 16.8‰) (Figure 4). We can replicate the observed $\delta^{18}O$ and $\Delta^{17}O$ of shallow aquifer NO_3^- by solely mixing end-member atmospheric and nitrification sources, as all Mg^{2+}-HCO_3^- fluids plotted close to the predicted mixing line. Ca^{2+}-OH^- fluids plotted closer to the estimated nitrification source, which likely

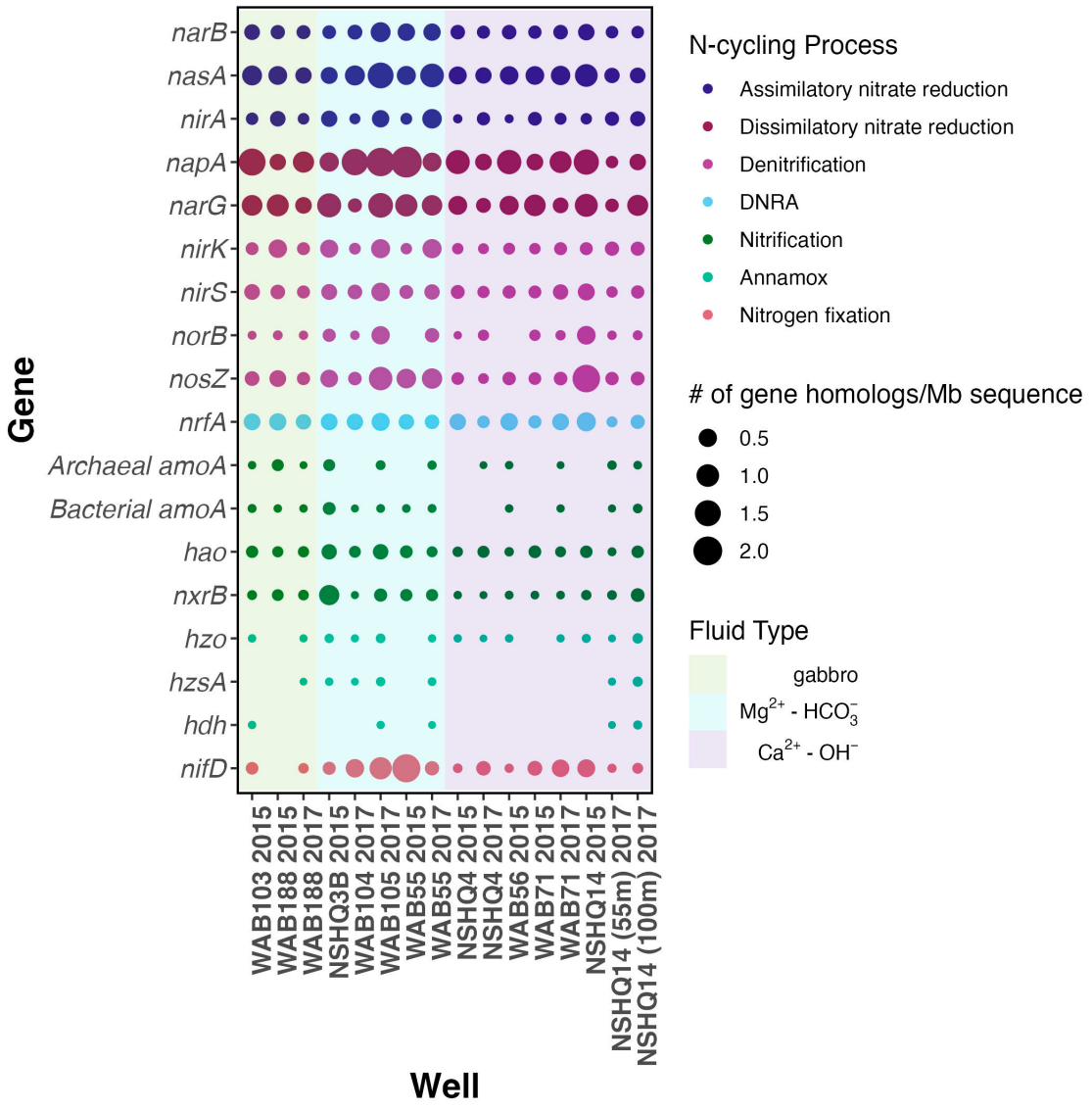

FIGURE 5
Dotplot of abundances of key N cycling genes, where the colors of the dots correspond to the type of N-cycling process, the size to the # of gene homologs detected per Mb sequence, and the background color representative of fluid type.

represents Ca^{2+}-OH^{-} fluids containing a greater proportion of nitrified NO_3^- than Mg^{2+}-HCO_3^- fluids.

4.3. NO_3^- is extensively reduced to NH_3 during progressive water–rock reaction

The concomitant decrease in NO_3^- concentration and increase in $\sum NH_3$ concentration with increasing pH (Figure 2) suggests a possible reduction of NO_3^- to $\sum NH_3$ during the progressive reaction of Mg^{2+}-HCO_3^- type fluids to reducing, Ca^{2+}-OH^{-} type fluids. We observed a trend of increasing $\delta^{15}N$ and $\delta^{18}O$ of NO_3^- with decreasing NO_3^- concentration (Figure 3) indicative of biological NR which characteristically enriches $\delta^{15}N$ and $\delta^{18}O$ of residual nitrate in approximately a 1:1 to 2:1 ratio (Casciotti and McIlvin, 2007; Casciotti et al., 2013; Gaye et al., 2013; Rafter et al., 2013; Bourbonnais et al., 2017). This trend implies ^{15}N isotopic discrimination of NR between −4.5‰ and −17.5‰ (Supplementary Figure 1) assuming Rayleigh kinetic fractionation dynamics. It is important to note that Samail Ophiolite aquifer fluids do not satisfy all assumptions for the Rayleigh fractionation model because nitrification and diffusion of NO_3^- from near-surface mixing may continually supply some NO_3^- during NO_3^- consumption.

In the Samail Ophiolite, reductants such as H_2 are produced during water-rock interactions, and most oxidants are highly limited in reacted hyperalkaline fluids. Thus, we would predict that NO_3^- introduced into the aquifer would act as an important electron acceptor for subsurface microbial metabolism. Accordingly, microbial NR through DNRA is a likely explanation for the presumed production of $\sum NH_3$ in

Samail Ophiolite aquifer fluids. DNRA is a common respiratory process in oligotrophic marine (Lam et al., 2009; Bonaglia et al., 2016), soil (Silver et al., 2001; Rütting et al., 2011; Zhang et al., 2015), and freshwater riparian to estuarine wetland environments (Welsh et al., 2001; Koop-Jakobsen and Giblin, 2010; Wang et al., 2020). The ubiquitous detection of *nrfA* gene homologs, the gene encoding the catalytic subunit for cytochrome c NO_2^- reductase for NO_2^- reduction to NH_4^+, further supports a biological role in the production of subsurface $\sum NH_3$.

While the isotope effect for DNRA has not been systematically evaluated, it is predicted to be similar to that of denitrification with an estimated maximum fractionation of ∼−30‰ (McCready et al., 2011). In both denitrification and DNRA, NO_3^- is first reduced by the periplasmic enzyme Nap (catalytic subunit encoded by *napA*) or the membrane-bound cytosolic enzyme Nar (catalytic subunit encoded by *narG*) which have $^{15}\varepsilon$ ranges of −11.4 to −39.8‰ and −6.6 to −31.6‰, respectively (Granger and Wankel, 2016; Asamoto et al., 2021; and references therein). There is an enzyme-specific coupling of O and N isotope fractionation during NR, with Nar reductases commonly imparting fractionation with a $^{18}\varepsilon/^{15}\varepsilon$ proportionality of approximately 0.91, and Nap reductases a $^{18}\varepsilon/^{15}\varepsilon$ proportionality of ∼ 0.55 (Asamoto et al., 2021). Accordingly, we presume if NR in Samail Ophiolite aquifer fluids is microbial, Nar reductases best explain the demonstrated proportionality of enrichment in $\delta^{18}O$ vs. $\delta^{15}N$ which was close to 1 (Figure 3). The observed discrimination for NR (−4.5 to −17.5‰) in Samail Ophiolite aquifers is largely consistent with dissimilatory NR with a Nar reductase, with reduced isotope effects due to NO_3^- uptake becoming the rate-limiting step at low concentrations of NO_3^- (Kritee et al., 2012) (see Supplementary datasheet). The predominance of Nap reductases in addition to Nar reductases in Samail Ophiolite aquifers could be explained by the functional diversity of Nap enzymes which can additionally be involved in the maintenance of cellular oxidation-reduction potential and NO_3^- scavenging (Potter and Cole, 1999; Potter et al., 1999; Richardson, 2000). Accordingly, the abundance of *napA* gene homologs does not necessarily indicate an active role in dissimilatory NR.

We do also consider that an abiotic reduction process could play a role in the conversion of NO_3^- to $\sum NH_3$. Although spontaneous NR in the presence of high H_2 concentrations is not expected to occur at the temperatures of the aquifer fluids (∼35° C), mineral-facilitated reduction by Fe-bearing phases could occur. For example, the quantitative conversion of NO_3^- to NH_4^+ can be catalyzed by green rust minerals at surface temperatures (Hansen et al., 1996). Similarly, Smirnov et al. (2008) reported the generation of NH_4^+ through NR in the presence of the FeNi alloys, such as awaruite ($Ni_{80}Fe_{20}$), although this reaction was highly temperature-dependent and proceeded almost negligibly at 22 °C (Smirnov et al., 2008). Yet, the detection of awaruite and Fe-bearing hydroxides in serpentinized peridotite in the Samail Ophiolite (Ellison et al., 2021) merits future investigation into the kinetics and associated isotope effects of these reactions under environmentally relevant conditions.

We note that other biological reduction pathways including denitrification to N_2 or assimilatory NR may have contributed to the observed NO_3^- consumption and loss from Samail Ophiolite aquifer fluids. We detected gene homologs for all major genes pertaining to denitrification (e.g., *nirS, nirK, norB,* and *nosZ*) (Philippot, 2002) in metagenomic sequencing of biomass from borehole fluids. High rates of denitrification have been reported in biological soil crusts in Oman associated with >300 μmol $N/m^2/h$ emissions of N_2O (Abed et al., 2013). We detected N_2O in nM concentrations (∼ 5–176 nM) in sampled aquifer fluids (Table 5). However, many other N cycling processes could produce N_2O, including the decomposition of intermediate hydroxylamine during NH_3 oxidation, reduction of NO_2^- by nitrifiers (nitrifier-denitrification), and reduction of NO_2^- through reaction with ferrous iron (chemodenitrification) (Wankel et al., 2017). Furthermore, DNRA would be expected to occur at higher rates than denitrification at alkaline pH (Yoon et al., 2015) and where NO_3^- is limited (Jørgensen, 1989; Kraft et al., 2014). In addition, the presence of assimilatory NR genes (e.g., *narB, nasA, nirA*) in aquifer fluids may indicate the potential for NR for assimilation into biomass instead of respiration (Moreno-Vivián et al., 1999); however, this process is unlikely to be the predominant NO_3^- consuming process in Ca^{2+}-OH^- type fluids where bioavailable N in the form of NH_3 is abundant and biomass is low (5×10^5 cells/mL) (Fones et al., 2019). The accompanying rise in $\sum NH_3$ concentrations with a decrease in NO_3^- concentrations and an increase in pH suggests that NR to $\sum NH_3$ is proportionally a more significant process, at least in Ca^{2+}-OH^- type fluids. However, additional measurements such as N_2/Ar ratios (Vogel et al., 1981), ^{15}N labeled assays, transcriptomics, and site-specific N_2O isotopic analyses should be carried out in future investigations of this system to more definitively assess the potential for alternative biological NR processes.

4.4. The isotopic composition of $\sum NH_3$ is highly variable in aquifer fluids

We observed a large range in $\delta^{15}N$ of $\sum NH_3$. We presume that $\delta^{15}N_{red}$ is equivalent to the $\delta^{15}N$ of $\sum NH_3$ for all boreholes except NSHQ14 and WAB188, as sampled fluids from these wells exhibited comparable N_{red} and $\sum NH_3$ concentrations (Table 3). The $\delta^{15}N < -12‰$ for $\sum NH_3$ measured in BA1A contrasts with positive values measured in other boreholes. This could be related to the collection of fluids with the packer system (see Supplementary datasheet), which discretely sampled the lower borehole (100–400 m), as this sampled pool of $\sum NH_3$ may reflect a pool that has undergone little oxidation by nitrifiers. The isotope effect for NH_3 oxidation can be as large as −38‰ for bacterial nitrification (Mariotti et al., 1981; Yoshida, 1988; Casciotti et al., 2003), and thus the partial oxidation of NH_3 in Ca^{2+}-OH^- fluids could enrich the residual $\sum NH_3$ pool, accounting in part for the higher $\delta^{15}N$ values of $\sum NH_3$ observed in other reacted fluids. In addition, there is a strong equilibrium isotope effect (−42.5‰) associated with $\sum NH_3$ speciation, volatilization, and degassing (Li et al., 2012). If ammonia is lost through degassing, the residual pool of NH_4^+, and thus $\sum NH_3$, should become increasingly enriched in ^{15}N. Finally, some variability in the $\delta^{15}N$ of $\sum NH_3$ can be explained by groundwater age. The $\delta^{15}N$ of NO_3^- in atmospheric deposition has decreased by approximately 15‰ over the past century due to the Haber–Bosch effect of increased anthropogenic

inputs from fertilizers (Yang and Gruber, 2016). Because Ca^{2+}-OH^- fluids in Oman are pre–H-bomb (older than 1952), whereas Mg-HCO_3^- are estimated to be only 4–40 years old (Paukert Vankeuren et al., 2019), the $\delta^{15}N$ composition of source NO_3^- was not consistent across fluids.

4.5. Other potential sources of $\sum NH_3$

Common sources of $\sum NH_3$ in aquifer catchments such as remineralized organic matter, fertilizer, or wastewater (Kendall Carol, 1998) are unlikely for the Samail Ophiolite aquifer system. Due to the location of the Samail Ophiolite in the Omani desert, there is little agriculture or even human inhabitation in the catchments that supply the subsurface aquifer. Furthermore, N_{red} is within the standard error for measured $\sum NH_3$ in most aquifer fluids. Dissolved organic N constitutes on average >80% of total N in anthropogenic runoff (Jani et al., 2020), thus we posit there is little contribution to reduced N from these sources where inorganic forms of N are predominant (see Supplementary datasheet for the discussion of samples where $N_{red} >> \sum NH_3$).

A major potential source of $\sum NH_3$ to Samail Ophiolite aquifers could be atmospheric deposition. Unfortunately, we did not acidify an aliquot of rainwater for analysis during the one rain event that coincided with our geochemical sampling, so the assessment of wet deposition was not possible. Whether through wet or dry deposition, atmospheric $\sum NH_3$ could be effectively transported to the subsurface aquifer through rainfall. However, despite the apparent atmospheric source for a significant fraction of shallow aquifer NO_3^-, the same cannot be presumed for $\sum NH_3$ because the atmospheric deposition of reduced nitrogen species (NH_x) is not necessarily correlated with the magnitude of N-oxide deposition. Sources of oxidized and reduced N in the atmosphere are quite different, with NH_x primarily originating from agricultural pollution such as emissions from livestock and volatilization of fertilizers (Reis et al., 2009).

Another source of $\sum NH_3$ to subsurface aquifers is biological N fixation. Although nitrogenase enzymes require high energetic costs to reduce N_2 gas to NH_4^+ (Broda and Peschek, 1980), this process has been hypothesized to occur in some oligotrophic, rock-hosted environments such as the Henderson Mine and the serpentinite-hosted Lost City hydrothermal field (Sahl et al., 2008; Swanner and Templeton, 2011; Lang et al., 2013). While we did detect *nifD* gene homologs (which encode the catalytic site for the nitrogenase enzyme), their detection did not correlate with $\sum NH_3$ concentrations. Alternatively, surficial $\sum NH_3$ produced by diazotrophic biological soil crusts could be transferred to the subsurface *via* recharging rainfall. N fixation by soil crusts commonly occurs in arid ecosystems, including Oman (Abed et al., 2010, 2013); however, aquifers in the Samail Ophiolite are hosted in alluvium and mafic to ultramafic bedrock without soil cover (Dewandel et al., 2005), likely limiting fixed soil N contributions to the aquifer. Regardless of where N fixation may occur, the fractionation imparted by nitrogenases cannot fully account for the ~30‰ variation in or the lowest (−16.7‰) $\delta^{15}N$ of $\sum NH_3$ observed. N fixation with common molybdenum–based nitrogenase enzymes only imparts a small isotopic effect of −2 to +1‰ (Macko et al., 1987), and less efficient vanadium and iron–based alternative nitrogenase enzymes a fractionation of −6 to −8‰ (Zhang et al., 2014). Accordingly, while N fixation may contribute $\sum NH_3$ to aquifer fluids, it seems unlikely as the primary source for the >100 μM $\sum NH_3$ observed in some Ca^{2+}-OH^- fluids.

Alternatively, rock-hosted N could be released during water–rock weathering reactions (Houlton et al., 2018). Although unaltered lithospheric peridotite has been found to have exceedingly low N concentrations (<1 ppm) (Yokochi et al., 2009), the substitution of NH_4^+ for potassium, calcium, or sodium in silicate minerals occurs widely (Holloway and Dahlgren, 2002), particularly as a result of water/rock interaction. We measured up to 13.9 ppm bulk N in serpentinized peridotite, which is within the range of concentrations (~1–20 ppm) measured for altered ophiolitic glasses (Bebout et al., 2017) and serpentinized metaperidotites (Philippot et al., 2007; Halama et al., 2010), where N is presumed to occur as silicate-bound NH_4^+ or trapped in fluid inclusions in sealed fractures produced during serpentinization reactions. Bulk $\delta^{15}N$ of our measured peridotite samples varied from 3.5 to 6.7‰, similar to values observed in altered basalts and peridotites (Busigny et al., 2005; Philippot et al., 2007; Halama et al., 2010; Bebout et al., 2017) and consistent of a mantle signature with some incorporation of NH_4^+ from reacted fluids (Busigny and Bebout, 2013). It is unclear whether the incorporation of NH_4^+ is ongoing through modern water–rock interactions, or if this N could be released into the fluids during rock dissolution. Future studies should investigate the potential for leaching of NH_4^+ from serpentinized peridotite, especially because on a microscale, fluid compositions in porewaters could be differentially enriched in dissolved N through this mechanism.

4.6. Recycling of $\sum NH_3$ in the near surface

NH_4^+ produced *via* DNRA in reacted fluids, in combination with $\sum NH_3$ from any aforementioned source, is recycled in the near surface through nitrification. Despite the highly reducing nature of Ca^{2+}-OH^- fluids (Eh typically below −100 mV), evidence for aerobic nitrification can be observed in some boreholes such as WAB71 where the $\delta^{18}O$ of NO_3^- measured was <10‰ across multiple years of sampling (Table 2). Nitrification is capable of proceeding at dissolved oxygen concentrations of 5–30 nM, or ~0.01% air saturation (Bristow et al., 2016), and thus NH_3 oxidation could occur in the shallow aquifer where Ca^{2+}-OH^- fluids come in contact with the atmosphere or mix with Mg-HCO_3^- type fluids.

Overall, the reduction of NO_3^- to NH_4^+, as opposed to N_2O or N_2 gas, retains N in the subsurface aquifer, thus preventing N from acting as a limiting nutrient for biological growth. The oxidation of $\sum NH_3$ produced by the reduction of atmospheric NO_3^- through nitrification would then allow for further recycling of N in the subsurface, serpentinite-hosted aquifer ecosystem to sustain microbial growth even when the aquifers are not actively recharged. This continued cycling of atmospherically sourced NO_3^- lends credence to the potential habitability of rock-hosted subsurface environments on other planetary bodies, such as Mars,

where surficial inputs of NO_3^- have been detected (Stern et al., 2017).

5. Conclusion

We employed dual N and O isotopic analysis of dissolved N species to probe the origin and subsequent cycling of NO_3^- in Samail Ophiolite aquifer fluids since NO_3^- is predicted to be a key electron acceptor for subsurface microbial life in terrestrial serpentinite ecosystems. NO_3^- in all measured aquifer fluids was characterized by a positive $\Delta^{17}O$ indicative of atmospheric deposition as a major source of oxidized N to the serpentinite-hosted aquifers. The $\Delta^{17}O$ and $\delta^{18}O$ of NO_3^- in shallow aquifer fluids were consistent with simple mixing of NO_3^- from atmospheric deposition with NO_3^- produced *via* nitrification. However, NO_3^- presumed to have formed through nitrification varied considerably in $\delta^{15}N$. In part, this is due to the ~30‰ variation of reactant $\sum NH_3$. Concentrations of $\sum NH_3$ increased concomitantly with a decrease in the concentration of NO_3^- in more deeply sourced fluids, implying that NR could be a major source of $\sum NH_3$ detected in Ca^{2+}-OH^- fluids. The isotopic fractionation imparted by NR seemingly varied with NO_3^- concentration, with greater fractionation ($\varepsilon^{15} \sim -17.5$‰) observed in shallow groundwaters, and less apparent fractionation ($\varepsilon^{15} \sim -4.5$‰) in deeper groundwaters where NO_3^- concentrations were $<30\,\mu M$. This difference in isotope effect could be explained if NO_3^- uptake becomes the rate-limiting step in NR in highly reacted fluids where NO_3^- is scarce. The relationship between O and N isotopic fractionation ($^{18}\varepsilon/^{15}\varepsilon$) during NO_3^- consumption was consistent with biological dissimilatory NR with a Nar reductase, although the possibility for abiotic reduction cannot be ruled out. Overall, the measured O and N isotopic compositions of NO_3^- in Samail Ophiolite aquifer fluids are consistent with the recycling of atmospherically derived N through the initial reduction of meteoric NO_3^- to NH_4^+ followed by partial (re)oxidation to NO_3^- during nitrification in the near surface. This mode of biogeochemical cycling has major implications for the habitability of these aquifers, as the reduction of NO_3^- to NH_4^+ retains N in the subsurface ecosystem.

Data availability statement

Raw isotopic data presented in this study and source code used to produce the figures and data tables in this manuscript are available at https://github.com/KopfLab/OmanN_Cycling. Metagenomic sequence files are available from the MG-RAST database under accession numbers mgm4795805.3 to mgm4795809.3 and mgm4795811.3.

Author contributions

AT, SK, JM, JS, and KR conceived the study. KR, DN, EK, JM, JS, and AT collected samples in the field. KR, DN, EK, CA, RDE, and SK analyzed samples and assisted in the data interpretation. KR wrote the manuscript. All authors critically revised the manuscript text and figures.

Funding

This research was directly supported by the Rock-Powered Life NASA Astrobiology Institute (NNA15BB02A). Samples were additionally provided by the Oman Drilling Project. The Oman Drilling Project is supported through combined funds from the International Continental Scientific Drilling Project, the Sloan Foundation–Deep Carbon Observatory (Grant 2014-3), the National Science Foundation (NSF-EAR), the NASA Astrobiology Institute (NNA15BB02A), the German Research Foundation (DFG), the Japanese Society for the Promotion of Science (JSPS), the European Research Council, the Swiss National Science Foundation, JAMSTEC, the TAMU-JR Science operator, and contributions from the Sultanate of Oman Ministry of Regional Municipalities and Water Resources, the Oman Public Authority of Mining, Sultan Qaboos University, CRNS-Univ. Montpellier II, Columbia University, and the University of Southampton.

Acknowledgments

We thank the Ministry of Regional Municipalities and Water Resources in the Sultanate of Oman for permits and access to boreholes for fluid sampling and export, the Oman Drilling Project for access to the Multi-Borehole Observatory, and Eric Ellison, Eric Boyd, Laura Bueter, and Lauren Seyler for assistance in field sampling. We would like to thank Daniel Sigman for access to analytical equipment at Princeton University and the entire Sigman Lab for support during isotopic analyses. In particular, we thank Emma Kast, Victoria Luu, Dario Marconi, Alexa Weigand, and Sergey Oleynik for guidance during sample preparation and assistance with isotopic measurements. We thank the Stüeken Lab at St. Andrews for the analysis of bulk $\delta^{15}N$ in peridotite rock, especially Toby Boocock for running the analyses, the Repert lab at the Boulder USGS offices for access to facilities for quantifying N_2O, and Benjamin Harlow at the Stable Isotope Core Lab at Washington State University for running the thermal decomposition triple oxygen isotopic analyses of nitrate. In addition, we thank Saroj Poudel for guidance in nitrogen functional gene analysis, Ben Johnson for discussions regarding rock-hosted nitrogen and arranging preliminary bulk $\delta^{15}N$ measurements with the Stüeken Lab, as well as Meaghan Petix and Katherine Gale for providing helpful comments to improve the manuscript.

Conflict of interest

The authors declare that the research was conducted in the absence of any commercial or financial relationships that could be construed as a potential conflict of interest.

Publisher's note

All claims expressed in this article are solely those of the authors and do not necessarily represent those of

their affiliated organizations, or those of the publisher, the editors and the reviewers. Any product that may be evaluated in this article, or claim that may be made by its manufacturer, is not guaranteed or endorsed by the publisher.

Supplementary material

The Supplementary Material for this article can be found online at: https://www.frontiersin.org/articles/10.3389/fmicb.2023.1139633/full#supplementary-material

References

Abed, R. M. M., Al Kharusi, S., Schramm, A., and Robinson, M. D. (2010). Bacterial diversity, pigments and nitrogen fixation of biological desert crusts from the Sultanate of Oman. *FEMS Microbiol. Ecol.* 72, 418–428. doi: 10.1111/j.1574-6941.2010.00854.x

Abed, R. M. M., Lam, P., de Beer, D., and Stief, P. (2013). High rates of denitrification and nitrous oxide emission in arid biological soil crusts from the Sultanate of Oman. *ISME J.* 7, 1862–1875. doi: 10.1038/ismej.2013.55

Andersson, K. K., and Hooper, A. B. (1983). O2 and H2O are each the source of one O in NO−2 produced from NH3 by Nitrosomonas: 15N-NMR evidence. *FEBS Lett.* 164, 236–240. doi: 10.1016/0014-5793(83)80292-0

Asamoto, C. K., Rempfert, K. R., Luu, V. H., Younkin, A. D., and Kopf, S. H. (2021). Enzyme-Specific Coupling of Oxygen and Nitrogen Isotope Fractionation of the Nap and Nar Nitrate Reductases. *Environ. Sci. Technol.* doi: 10.1021/acs.est.0c07816

Avanzino, R. J., and Kennedy, V. C. (1993). Long-term frozen storage of stream water samples for dissolved orthophosphate, nitrate plus nitrite, and ammonia analysis. *Water Resour. Res.* 29, 3357–3362. doi: 10.1029/93WR01684

Barnes, I., LaMarche, V. C., and Himmelberg, G. (1967). Geochemical evidence of present-day serpentinization. *Science.* 156, 830–832. doi: 10.1126/science.156.3776.830

Barnes, I., and O'neil, J. R. (1969). The relationship between fluids in some fresh alpine-type ultramafics and possible modern serpentinization, Western United States. *Geol. Soc. Am. Bull.* 80, 1947–1960. doi: 10.1130/0016-7606(1969)801947:TRBFIS2.0.CO;2

Bates, S. T., Berg-Lyons, D., Caporaso, J. G., Walters, W. A., Knight, R., and Fierer, N. (2011). Examining the global distribution of dominant archaeal populations in soil. *ISME J.* 5, 908–917. doi: 10.1038/ismej.2010.171

Bebout, G. E., Banerjee, N. R., Izawa, M. R. M., Kobayashi, K., Lazzeri, K., Ranieri, L. A. (2017). Nitrogen concentrations and isotopic compositions of seafloor-altered terrestrial basaltic glass: implications for astrobiology. *Astrobiology.* 18, 330–342. doi: 10.1089/ast.2017.1708

Bebout, G. E., Idleman, B. D., Li, L., and Hilkert, A. (2007). Isotope-ratio-monitoring gas chromatography methods for high-precision isotopic analysis of nanomole quantities of silicate nitrogen. *Chem. Geol.* 240, 1–10. doi: 10.1016/j.chemgeo.2007.01.006

Böhlke, J. K., Ericksen, G. E., and Revesz, K. (1997). Stable isotope evidence for an atmospheric origin of desert nitrate deposits in northern Chile and southern California, U.S.A. *Chem. Geol.* 136, 135–152. doi: 10.1016/S0009-2541(96)00124-6

Bonaglia, S., Klawonn, I., De Brabandere, L., Deutsch, B., Thamdrup, B., and Brüchert, V. (2016). Denitrification and DNRA at the Baltic Sea oxic-anoxic interface: Substrate spectrum and kinetics: denitrification and DNRA at the oxic-anoxic interface. *Limnol. Oceanogr.* 61, 1900–1915. doi: 10.1002/lno.10343

Boocock, T. J., Mikhail, S., Prytulak, J., Rocco, T. D., and Stüeken, E. E. (2020). Nitrogen mass fraction and stable isotope ratios for fourteen geological reference materials: evaluating the applicability of elemental analyser versus sealed tube combustion methods. *Geostand. Geoanalytical Res.* 44, 537–551. doi: 10.1111/ggr.12345

Boshers, D. S., Granger, J., Tobias, C. R., Böhlke, J. K., and Smith, R. L. (2019). Constraining the oxygen isotopic composition of nitrate produced by nitrification. *Environ. Sci. Technol.* 53, 1206–1216. doi: 10.1021/acs.est.8b03386

Böttcher, J., Strebel, O., Voerkelius, S., and Schmidt, H.-L. (1990). Using isotope fractionation of nitrate-nitrogen and nitrate-oxygen for evaluation of microbial denitrification in a sandy aquifer. *J. Hydrol.* 114, 413–424. doi: 10.1016/0022-1694(90)90068-9

Bourbonnais, A., Letscher, R. T., Bange, H. W., Échevin, V., Larkum, J., Mohn, J., et al. (2017). N2O production and consumption from stable isotopic and concentration data in the Peruvian coastal upwelling system. *Glob. Biogeochem. Cycles* 31, 678–698. doi: 10.1002/2016GB005567

Bristow, L. A., Dalsgaard, T., Tiano, L., Mills, D. B., Bertagnolli, A. D., Wright, J. J., et al. (2016). Ammonium and nitrite oxidation at nanomolar oxygen concentrations in oxygen minimum zone waters. *Proc. Natl. Acad. Sci.* 113, 10601–10606. doi: 10.1073/pnas.1600359113

Broda, E., and Peschek, G. A. (1980). Evolutionary considerations on the thermodynamics of nitrogen fixation. *Biosystems* 13, 47–56. doi: 10.1016/0303-2647(80)90004-0

Bruni, J., Canepa, M., Chiodini, G., Cioni, R., Cipolli, F., Longinelli, A., et al. (2002). Irreversible water–rock mass transfer accompanying the generation of the neutral, Mg–HCO3 and high-pH, Ca–OH spring waters of the Genova province, Italy. *Appl. Geochem.* 17, 455–474. doi: 10.1016/S0883-2927(01)00113-5

Buchfink, B., Xie, C., and Huson, D. H. (2015). Fast and sensitive protein alignment using DIAMOND. *Nat. Methods* 12, 59–60. doi: 10.1038/nmeth.3176

Buchwald, C., and Casciotti, K. L. (2010). Oxygen isotopic fractionation and exchange during bacterial nitrite oxidation. *Limnol. Oceanogr.* 55, 1064–1074. doi: 10.4319/lo.2010.55.3.1064

Buchwald, C., Santoro, A. E., McIlvin, M. R., and Casciotti, K. L. (2012). Oxygen isotopic composition of nitrate and nitrite produced by nitrifying cocultures and natural marine assemblages. *Limnol. Oceanogr.* 57, 1361–1375. doi: 10.4319/lo.2012.57.5.1361

Busigny, V., and Bebout, G. E. (2013). Nitrogen in the Silicate Earth: Speciation and Isotopic Behavior during Mineral–Fluid Interactions. *Elements* 9, 353–358. doi: 10.2113/gselements.9.5.353

Busigny, V., Laverne, C., and Bonifacie, M. (2005). Nitrogen content and isotopic composition of oceanic crust at a superfast spreading ridge: a profile in altered basalts from ODP Site (1256). Leg 206. Geochem. Geophys. Geosystems 6. doi: 10.1029/2005GC001020

Casciotti, K. L., Buchwald, C., and McIlvin, M. (2013). Implications of nitrate and nitrite isotopic measurements for the mechanisms of nitrogen cycling in the Peru oxygen deficient zone. *Deep Sea Res. Part Oceanogr. Res. Pap.* 80, 78–93. doi: 10.1016/j.dsr.2013.05.017

Casciotti, K. L., and McIlvin, M. R. (2007). Isotopic analyses of nitrate and nitrite from reference mixtures and application to Eastern Tropical North Pacific waters. *Mar. Chem.* 107, 184–201. doi: 10.1016/j.marchem.2007.06.021

Casciotti, K. L., Sigman, D. M., Hastings, M. G., Böhlke, J. K., and Hilkert, A. (2002). Measurement of the oxygen isotopic composition of nitrate in seawater and freshwater using the denitrifier method. *Anal. Chem.* 74, 4905–4912. doi: 10.1021/ac020113w

Casciotti, K. L., Sigman, D. M., and Ward, B. B. (2003). Linking diversity and stable isotope fractionation in ammonia-oxidizing bacteria. *Geomicrobiol. J.* 20, 335–353. doi: 10.1080/01490450303895

Chavagnac, V., Monnin, C., Ceuleneer, G., Boulart, C., and Hoareau, G. (2013). Characterization of hyperalkaline fluids produced by low-temperature serpentinization of mantle peridotites in the Oman and Ligurian ophiolites. *Geochem. Geophys. Geosystems* 14, 2496–2522. doi: 10.1002/ggge.20147

Chen, D. J. Z., and MacQuarrie, K. T. B. (2011). Correlation of δ15N and δ18O in NO3- during denitrification in groundwater. *J. Environ. Eng. Sci.* 4, 221–226. doi: 10.1139/s05-002

Daims, H., Lebedeva, E. V., Pjevac, P., Han, P., Herbold, C., Albertsen, M., et al. (2015). Complete nitrification by *Nitrospira bacteria*. *Nature.* 528, 504–509. doi: 10.1038/nature16461

Dejwakh, N. R., Meixner, T., Michalski, G., and McIntosh, J. (2012). Using 17O to investigate nitrate sources and sinks in a semi-arid groundwater system. *Environ. Sci. Technol.* 46, 745–751. doi: 10.1021/es203450z

Dewandel, B., Lachassagne, P., Boudier, F., Al-Hattali, S., Ladouche, B., Pinault, J.-L., et al. (2005). A conceptual hydrogeological model of ophiolite hard-rock aquifers in Oman based on a multiscale and a multidisciplinary approach. *Hydrogeol. J.* 13, 708–726. doi: 10.1007/s10040-005-0449-2

Dewandel, B., Lachassagne, P., and Qatan, A. (2004). Spatial measurements of stream baseflow, a relevant method for aquifer characterization and permeability evaluation. Application to a hard-rock aquifer, the Oman ophiolite. *Hydrol. Process.* 18, 3391–3400. doi: 10.1002/hyp.1502

Ellison, E. T., Templeton, A. S., Zeigler, S. D., Mayhew, L., Kelemen, P. B., and Matter, J. (2021). Iron mineralogy, hydrogen production, and brucite reactivity during

low-temperature serpentinization in the Samail ophiolite. *Journal of Geophysical Research: Solid Earth*. 126, e2021JB021981. doi: 10.1029/2021JB021981

Escudero, C., Oggerin, M., and Amils, R. (2018). The deep continental subsurface: the dark biosphere. *Int. Microbiol*. 21, 3–14. doi: 10.1007/s10123-018-0009-y

Ewing, S. A., Michalski, G., Thiemens, M., Quinn, R. C., Macalady, J. L., Kohl, S., et al. (2007). Rainfall limit of the N cycle on Earth. *Glob. Biogeochem. Cycles* 21. doi: 10.1029/2006GB002838

Flemming, H.-C., and Wuertz, S. (2019). Bacteria and archaea on Earth and their abundance in biofilms. *Nat. Rev. Microbiol*. 17, 247–260. doi: 10.1038/s41579-019-0158-9

Fones, E. M., Colman, D. R., Kraus, E. A., Nothaft, D. B., Poudel, S., Rempfert, K. R., et al. (2019). Physiological adaptations to serpentinization in the Samail Ophiolite, Oman. *ISME J*. 13, 1750–1762. doi: 10.1038/s41396-019-0391-2

García-Robledo, E., Corzo, A., and Papaspyrou, S. (2014). A fast and direct spectrophotometric method for the sequential determination of nitrate and nitrite at low concentrations in small volumes. *Mar. Chem*. 162, 30–36. doi: 10.1016/j.marchem.2014.03.002

Gaye, B., Nagel, B., Dähnke, K., Rixen, T., and Emeis, K.-C. (2013). Evidence of parallel denitrification and nitrite oxidation in the ODZ of the Arabian Sea from paired stable isotopes of nitrate and nitrite. *Glob. Biogeochem. Cycles*. 27, 1059–1071. doi: 10.1002/2011GB004115

Granger, J., and Sigman, D. M. (2009). Removal of nitrite with sulfamic acid for nitrate N and O isotope analysis with the denitrifier method. *Rapid Commun. Mass Spectrom*. 23, 3753–3762. doi: 10.1002/rcm.4307

Granger, J., Sigman, D. M., Lehmann, M. F., and Tortell, P. D. (2008). Nitrogen and oxygen isotope fractionation during dissimilatory nitrate reduction by denitrifying bacteria. *Limnol. Oceanogr*. 53, 2533–2545. doi: 10.4319/lo.2008.53.6.2533

Granger, J., and Wankel, S. D. (2016). Isotopic overprinting of nitrification on denitrification as a ubiquitous and unifying feature of environmental nitrogen cycling. *Proc. Natl. Acad. Sci*. 113, E6391–E6400. doi: 10.1073/pnas.1601383113

Halama, R., Bebout, G. E., John, T., and Schenk, V. (2010). Nitrogen recycling in subducted oceanic lithosphere: the record in high- and ultrahigh-pressure metabasaltic rocks. *Geochim. Cosmochim. Acta* 74, 1636–1652. doi: 10.1016/j.gca.2009.12.003

Hansen, H., Chr, B., Koch, C. B., Nancke-Krogh, H., Borggaard, O. K., and Sørensen, J. (1996). Abiotic nitrate reduction to ammonium: key role of green rust. *Environ. Sci. Technol*. 30, 2053–2056. doi: 10.1021/es950844w

Holloway, J. M., and Dahlgren, R. A. (2002). Nitrogen in rock: occurrences and biogeochemical implications. *Glob. Biogeochem. Cycles*. 16, 65-1 65–17. doi: 10.1029/2002GB001862

Houlton, B. Z., Morford, S. L., and Dahlgren, R. A. (2018). Convergent evidence for widespread rock nitrogen sources in Earth's surface environment. *Science* 360, 58–62. doi: 10.1126/science.aan4399

Jani, J., Yang, Y.-Y., Lusk, M. G., and Toor, G. S. (2020). Composition of nitrogen in urban residential stormwater runoff: concentrations, loads, and source characterization of nitrate and organic nitrogen. *PLoS ONE*. 15, e0229715. doi: 10.1371/journal.pone.0229715

Jones, R. M., Goordial, J. M., and Orcutt, B. N. (2018). low energy subsurface environments as extraterrestrial analogs. *Front. Microbiol*. 9, 01605. doi: 10.3389/fmicb.2018.01605

Jørgensen, K. S. (1989). Annual pattern of denitrification and nitrate ammonification in estuarine sediment. *Appl. Environ. Microbiol*. 55, 1841–1847. doi: 10.1128/aem.55.7.1841-1847.1989

Kaiser, J., Hastings, M. G., Houlton, B. Z., Röckmann, T., and Sigman, D. M. (2007). Triple oxygen isotope analysis of nitrate using the denitrifier method and thermal decomposition of N2O. *Anal. Chem*. 79, 599–607. doi: 10.1021/ac061022s

Kartal, B., Kuypers, M. M. M., Lavik, G., Schalk, J., Camp, H. J. M. O., den, Jetten, M. S. M., et al. (2007). Anammox bacteria disguised as denitrifiers: nitrate reduction to dinitrogen gas via nitrite and ammonium. *Environ. Microbiol*. 9, 635–642. doi: 10.1111/j.1462-2920.2006.01183.x

Kaushal, S. S., Groffman, P. M., Band, L. E., Elliott, E. M., Shields, C. A., and Kendall, C. (2011). Tracking nonpoint source nitrogen pollution in human-impacted watersheds. *Environ. Sci. Technol*. 45, 8225–8232. doi: 10.1021/es200779e

Kelemen, P. B., Matter, J. M., Teagle, D. A. H., Coggon, J. A., and Oman Drilling Project Science Team (2020). *Oman Drilling Project, Scientific Drilling in the Samail Ophiolite*. Sultanate of Oman: WWW Document.

Kendall Carol (1998). "Chapter 16 - Tracing Nitrogen Sources and Cycling in Catchments", in *Isotope Tracers in Catchment Hydrology*, Kendall, C., and McDONNELL, J.J. (eds.). Amsterdam: Elsevier.p. 519–576. doi: 10.1016/B978-0-444-81546-0.50023-9

Kendall, C., Elliott, E. M., and Wankel, S. D. (2007). "Tracing Anthropogenic Inputs of Nitrogen to Ecosystems", in *Stable Isotopes in Ecology and Environmental Science*. New York, NY: John Wiley and Sons, Ltd. p. 375–449. doi: 10.1002/9780470691854.ch12

Knöller, K., Vogt, C., Haupt, M., Feisthauer, S., and Richnow, H.-H. (2011). Experimental investigation of nitrogen and oxygen isotope fractionation in nitrate and nitrite during denitrification. *Biogeochemistry*. 103, 371–384. doi: 10.1007/s10533-010-9483-9

Komatsu, D. D., Ishimura, T., Nakagawa, F., and Tsunogai, U. (2008). Determination of the 15N/14N, 17O/16O, and 18O/16O ratios of nitrous oxide by using continuous-flow isotope-ratio mass spectrometry. *Rapid Commun. Mass Spectrom. RCM*. 22, 1587–1596. doi: 10.1002/rcm.3493

Koop-Jakobsen, K., and Giblin, A. E. (2010). The effect of increased nitrate loading on nitrate reduction via denitrification and DNRA in salt marsh sediments. *Limnol. Oceanogr*. 55, 789–802. doi: 10.4319/lo.2010.55.2.0789

Kraft, B., Tegetmeyer, H. E., Sharma, R., Klotz, M. G., Ferdelman, T. G., Hettich, R. L., et al. (2014). The environmental controls that govern the end product of bacterial nitrate respiration. *Science*. 345, 676–679. doi: 10.1126/science.1254070

Kraus, E. A., Nothaft, D., Stamps, B. W., Rempfert, K. R., Ellison, E. T., Matter, J. M., et al. (2021). Molecular evidence for an active microbial methane cycle in subsurface serpentinite-hosted groundwaters in the samail ophiolite, Oman. *Appl. Environ. Microbiol*. 87, e02068–20. doi: 10.1128/AEM.02068-20

Kritee, K., Sigman, D. M., Granger, J., Ward, B. B., Jayakumar, A., and Deutsch, C. (2012). Reduced isotope fractionation by denitrification under conditions relevant to the ocean. *Geochim. Cosmochim. Acta* 92, 243–259. doi: 10.1016/j.gca.2012.05.020

Lam, P., Lavik, G., Jensen, M. M., Vossenberg, J., van de, Schmid, M., Woebken, D., et al. (2009). Revising the nitrogen cycle in the Peruvian oxygen minimum zone. *Proc. Natl. Acad. Sci*. 106, 4752–4757. doi: 10.1073/pnas.0812444106

Lang, S. Q., Früh-Green, G. L., Bernasconi, S. M., and Butterfield, D. A. (2013). Sources of organic nitrogen at the serpentinite-hosted Lost City hydrothermal field. *Geobiology*. 11, 154–169. doi: 10.1111/gbi.12026

Lehtovirta-Morley, L. E. (2018). Ammonia oxidation: ecology, physiology, biochemistry and why they must all come together. *FEMS Microbiol. Lett*. 365, 9. doi: 10.1093/femsle/fny058

Leong, J. A. M., Howells, A. E., Robinson, K. J., Cox, A., Debes, R. V., Fecteau, K., et al. (2021). Theoretical predictions vs environmental observations on serpentinization fluids: Lessons from the Samail ophiolite in Oman [WWW Document]. *J. Geophy Reseach: Solid Earth*. 126, e2020JB020756.

Leong, J. A. M., and Shock, E. L. (2020). Thermodynamic constraints on the geochemistry of low-temperature, continental, serpentinization-generated fluids. *Am. J. Sci*. 320, 185–235. doi: 10.2475/03.2020.01

Li, K., Liu, X., Song, W., Chang, Y., Hu, Y., and Tian, C. (2013). Atmospheric nitrogen deposition at two sites in an arid environment of Central Asia. *PLoS ONE*. 8, e67018. doi: 10.1371/journal.pone.0067018

Li, L., Lollar, B. S., Li, H., Wortmann, U. G., and Lacrampe-Couloume, G. (2012). Ammonium stability and nitrogen isotope fractionations for NH4+-NH3(aq)–NH3(gas) systems at 20–70°C and pH of 2–13: applications to habitability and nitrogen cycling in low-temperature hydrothermal systems. *Geochim. Cosmochim. Acta*. 84, 280–296. doi: 10.1016/j.gca.2012.01.040

Lods, G., Roubinet, D., Matter, J. M., LEPROVOST, R., and Gouze, P. (2020). Groundwater flow characterization of an ophiolitic hard-rock aquifer from cross-borehole multi-level hydraulic experiments. *J. Hydrol*. 589, 125152. doi: 10.1016/j.jhydrol.2020.125152

Loganathan, N., and Kalinichev, A. G. (2013). On the hydrogen bonding structure at the aqueous interface of ammonium-substituted mica: a molecular dynamics simulation. *Z. Für Naturforschung A*. 68, 91–100. doi: 10.5560/zna.2012-0101

Lybrand, R. A., Michalski, G., Graham, R. C., and Parker, D. R. (2013). The geochemical associations of nitrate and naturally formed perchlorate in the Mojave Desert, California, USA. *Geochim. Cosmochim. Acta*. 104, 136–147. doi: 10.1016/j.gca.2012.10.028

Lyons, J. R. (2001). Transfer of mass-independent fractionation in ozone to other oxygen-containing radicals in the atmosphere. *Geophys. Res. Lett*. 28, 3231–3234. doi: 10.1029/2000GL012791

Maalcke, W. J., Reimann, J., de Vries, S., Butt, J. N., Dietl, A., Kip, N., et al. (2016). Characterization of anammox hydrazine dehydrogenase, a key N2-producing enzyme in the global nitrogen cycle. *J. Biol. Chem*. 291, 17077–17092. doi: 10.1074/jbc.M116.735530

Macko, S. A., Fogel, M. L., Hare, P. E., and Hoering, T. C. (1987). Isotopic fractionation of nitrogen and carbon in the synthesis of amino acids by microorganisms. *Chem. Geol. Isot. Geosci. Sect*. 65, 79–92. doi: 10.1016/0168-9622(87)90064-9

Magnabosco, C., Lin, L.-H., Dong, H., Bomberg, M., Ghiorse, W., Stan-Lotter, H., et al. (2018). The biomass and biodiversity of the continental subsurface. *Nat. Geosci*. 11, 707–717. doi: 10.1038/s41561-018-0221-6

Mariotti, A., Germon, J. C., Hubert, P., Kaiser, P., Letolle, R., Tardieux, A., et al. (1981). Experimental determination of nitrogen kinetic isotope fractionation: some principles; illustration for the denitrification and nitrification processes. *Plant Soil*. 62, 413–430. doi: 10.1007/BF02374138

Martens-Habbena, W., Berube, P. M., Urakawa, H., de la Torre, J. R., and Stahl, D. A. (2009). Ammonia oxidation kinetics determine niche separation of nitrifying Archaea and Bacteria. *Nature*. 461, 976–979. doi: 10.1038/nature08465

Mauersberger, K., Lämmerzahl, P., and Krankowsky, D. (2001). Stratospheric ozone isotope enrichments—revisited. *Geophys. Res. Lett.* 28, 3155–3158. doi: 10.1029/2001GL013439

McCollom, T. M., and Bach, W. (2009). Thermodynamic constraints on hydrogen generation during serpentinization of ultramafic rocks. *Geochim. Cosmochim. Acta.* 73, 856–875. doi: 10.1016/j.gca.2008.10.032

McCready, R. G. L., Gould, W. D., and Barendregt, R. W. (2011). Nitrogen isotope fractionation during the reduction of NO3– to NH4+ by Desulfovibrio sp. *Can. J. Microbiol.* 29, 231–234. doi: 10.1139/m83-038

Menchyk, N., Park, D., Moon, P. H., Unruh, J. B., and Trenholm, L. E. (2014). Freezing low volume aqueous solutions to preserve ammonia and nitrate plus nitrite. *Crop Sci.* 54, 2325–2327. doi: 10.2135/cropsci2013.12.0807

Meyer-Dombard, D. R., and Malas, J. (2022). Advances in defining ecosystem functions of the terrestrial subsurface biosphere. *Front. Microbiol.* 13, 891528. doi: 10.3389/fmicb.2022.891528

Michalski, G., Bhattacharya, S. K., and Mase, D. F. (2012). "Oxygen Isotope Dynamics of Atmospheric Nitrate and Its Precursor Molecules", in *Handbook of Environmental Isotope Geochemistry: Vol I, Advances in Isotope Geochemistry,* Baskaran, M. (ed.). Berlin, Heidelberg: Springer. p. 613–635. doi: 10.1007/978-3-642-10637-8_30

Michalski, G., Böhlke, J. K., and Thiemens, M. (2004). Long term atmospheric deposition as the source of nitrate and other salts in the Atacama Desert, Chile: New evidence from mass-independent oxygen isotopic compositions. *Geochim. Cosmochim. Acta* 68, 4023–4038. doi: 10.1016/j.gca.2004.04.009

Michalski, G., Savarino, J., Böhlke, J. K., and Thiemens, M. (2002). Determination of the total oxygen isotopic composition of nitrate and the calibration of a Δ17? nitrate reference material. *Anal. Chem.* 74, 4989–4993. doi: 10.1021/ac0256282

Michalski, G., Scott, Z., Kabiling, M., and Thiemens, M. H. (2003). First measurements and modeling of Δ17O in atmospheric nitrate. *Geophys. Res. Lett.* 30. doi: 10.1029/2003GL017015

Miller, M. F. (2002). Isotopic fractionation and the quantification of 17O anomalies in the oxygen three-isotope system: an appraisal and geochemical significance. *Geochim. Cosmochim. Acta* 66, 1881–1889. doi: 10.1016/S0016-7037(02)00832-3

Moreno-Vivián, C., Cabello, P., Martínez-Luque, M., Blasco, R., and Castillo, F. (1999). Prokaryotic nitrate reduction: molecular properties and functional distinction among bacterial nitrate reductases. *J. Bacteriol.* 181, 6573–6584. doi: 10.1128/JB.181.21.6573-6584.1999

Mosley, O. E., Gios, E., Close, M., Weaver, L., Daughney, C., and Handley, K. M. (2022). Nitrogen cycling and microbial cooperation in the terrestrial subsurface. *ISME J.* 16, 2561–2573. doi: 10.1038/s41396-022-01300-0

Mysen, B. (2019). Nitrogen in the Earth: abundance and transport. *Prog. Earth Planet. Sci.* 6, 38. doi: 10.1186/s40645-019-0286-x

Nicolas, A., Boudier, F., Ildefonse, B., and Ball, E. (2000). Accretion of Oman and United Arab Emirates ophiolite – Discussion of a new structural map. *Mar. Geophys. Res.* 21, 147–180. doi: 10.1023/A:1026769727917

Nothaft, D., Templeton, A. S., Boyd, E., Matter, J., Stute, M., and Vankeuren, A. N. P. (2021). Aqueous geochemical and microbial variation across discrete depth intervals in a peridotite aquifer assessed using a packer system in the Samail Ophiolite, Oman. *Jour of Geophy Research: Solid Earth.* 126, e2021JG006319. doi: 10.1029/2021JG006319

Nyyssönen, M., Hultman, J., Ahonen, L., Kukkonen, I., Paulin, L., Laine, P., et al. (2014). Taxonomically and functionally diverse microbial communities in deep crystalline rocks of the Fennoscandian shield. *ISME J.* 8, 126–138. doi: 10.1038/ismej.2013.125

Paukert Vankeuren, A. N., Matter, J. M., Stute, M., and Kelemen, P. B. (2019). Multitracer determination of apparent groundwater ages in peridotite aquifers within the Samail ophiolite, Sultanate of Oman. *Earth Planet. Sci. Lett.* 516, 37–48. doi: 10.1016/j.epsl.2019.03.007

Paukert, A. N., Matter, J. M., Kelemen, P. B., Shock, E. L., and Havig, J. R. (2012). Reaction path modeling of enhanced in situ CO2 mineralization for carbon sequestration in the peridotite of the Samail Ophiolite, Sultanate of Oman. Chem. Geol. 330–331, 86–100. doi: 10.1016/j.chemgeo.2012.08.013

Philippot, L. (2002). Denitrifying genes in bacterial and archaeal genomes. *Biochim. Biophys. Acta BBA - Gene Struct. Expr.* 1577, 355–376. doi: 10.1016/S0167-4781(02)00420-7

Philippot, P., Busigny, V., Scambelluri, M., and Cartigny, P. (2007). Oxygen and nitrogen isotopes as tracers of fluid activities in serpentinites and metasediments during subduction. *Mineral. Petrol.* 91, 11–24. doi: 10.1007/s00710-007-0183-7

Potter, L. C., and Cole, J. A. (1999). Essential roles for the products of the napABCD genes, but not napFGH, in periplasmic nitrate reduction by Escherichia coli K-12. *Biochem. J.* 344, 69–76. doi: 10.1042/bj3440069

Potter, L. C., Millington, P., Griffiths, L., Thomas, G. H., and Cole, J. A. (1999). Competition between Escherichia coli strains expressing either a periplasmic or a membrane-bound nitrate reductase: does Nap confer a selective advantage during nitrate-limited growth? *Biochem. J.* 344, 77–84. doi: 10.1042/bj3440077

Rafter, P. A., DiFiore, P. J., and Sigman, D. M. (2013). Coupled nitrate nitrogen and oxygen isotopes and organic matter remineralization in the Southern and Pacific Oceans. *J. Geophys. Res. Oceans* 118, 4781–4794. doi: 10.1002/jgrc.20316

Reis, S., Pinder, R. W., Zhang, M., Lijie, G., and Sutton, M. A. (2009). Reactive nitrogen in atmospheric emission inventories. *Atmospheric Chem. Phys.* 9, 7657–7677. doi: 10.5194/acp-9-7657-2009

Rempfert, K. R., Miller, H. M., Bompard, N., Nothaft, D., Matter, J. M., Kelemen, P., et al. (2017). Geological and geochemical controls on subsurface microbial life in the samail ophiolite, Oman. *Front. Microbiol.* 8, 00056. doi: 10.3389/fmicb.2017.00056

Repert, D. A., Underwood, J. C., Smith, R. L., and Song, B. (2014). Nitrogen cycling processes and microbial community composition in bed sediments in the Yukon River at Pilot Station. *J. Geophys. Res. Biogeosciences.* 119, 2328–2344. doi: 10.1002/2014JG002707

Richardson, D. J. (2000). Bacterial respiration: a flexible process for a changing environment. *Microbiol. Read. Engl.* 146, 551–571. doi: 10.1099/00221287-146-3-551

Riha, K. M., Michalski, G., Gallo, E. L., Lohse, K. A., Brooks, P. D., and Meixner, T. (2014). High atmospheric nitrate inputs and nitrogen turnover in semi-arid urban catchments. *Ecosystems.* 17, 1309–1325. doi: 10.1007/s10021-014-9797-x

Ruppersberg, H. S., Goebel, M. R., Kleinert, S. I., Wünsch, D., Trautwein, K., and Rabus, R. (2017). Photometric determination of ammonium and phosphate in seawater medium using a microplate reader. *Microb. Physiol.* 27, 73–80. doi: 10.1159/000454814

Rütting, T., Boeckx, P., Müller, C., and Klemedtsson, L. (2011). Assessment of the importance of dissimilatory nitrate reduction to ammonium for the terrestrial nitrogen cycle. *Biogeosciences.* 8, 1779–1791. doi: 10.5194/bg-8-1779-2011

Sabuda, M. C., Brazelton, W. J., Putman, L. I., McCollom, T. M., Hoehler, T. M., Kubo, M. D. Y., et al. (2020). A dynamic microbial sulfur cycle in a serpentinizing continental ophiolite. *Environ. Microbiol.* 22, 2329–2345. doi: 10.1111/1462-2920.15006

Sahl, J. W., Schmidt, R., Swanner, E. D., Mandernack, K. W., Templeton, A. S., Kieft, T. L., et al. (2008). Subsurface microbial diversity in deep-granitic-fracture water in Colorado. *Appl. Environ. Microbiol.* 74, 143–152. doi: 10.1128/AEM.01133-07

Saud, S., Fahad, S., and Hassan, S. (2022). Developments in the investigation of nitrogen and oxygen stable isotopes in atmospheric nitrate. *Sustain. Chem. Clim. Action.* 1, 100003. doi: 10.1016/j.scca.2022.100003

Savard, M. M., Cole, A. S., Vet, R., and Smirnoff, A. (2018). The $\Delta^{17}O$ and $\delta^{18}O$ values of atmospheric nitrates simultaneously collected downwind of anthropogenic sources – implications for polluted air masses. *Atmospheric Chem. Phys.* 18, 10373–10389. doi: 10.5194/acp-18-10373-2018

Savarino, J., Bhattacharya, S. K., Morin, S., Baroni, M., and Doussin, J.-F. (2008). The NO+O3 reaction: a triple oxygen isotope perspective on the reaction dynamics and atmospheric implications for the transfer of the ozone isotope anomaly. *J. Chem. Phys.* 128, 194303. doi: 10.1063/1.2917581

Savarino, J., Lee, C. C. W., and Thiemens, M. H. (2000). Laboratory oxygen isotopic study of sulfur (IV) oxidation: origin of the mass-independent oxygen isotopic anomaly in atmospheric sulfates and sulfate mineral deposits on Earth. *J. Geophys. Res. Atmospheres* 105, 29079–29088. doi: 10.1029/2000JD900456

Schubert, M., Lindgreen, S., and Orlando, L. (2016). AdapterRemoval v2: rapid adapter trimming, identification, and read merging. *BMC Res. Notes.* 9, 88. doi: 10.1186/s13104-016-1900-2

Seyler, L. M., Brazelton, W. J., McLean, C., Putman, L. I., Hyer, A., Kubo, M. D. Y., et al. (2020). Carbon assimilation strategies in ultrabasic groundwater: clues from the integrated study of a serpentinization-influenced aquifer. *mSystems.* 5, e00607–19. doi: 10.1128/mSystems.00607-19

Sigman, D. M., Casciotti, K. L., Andreani, M., Barford, C., Galanter, M., and Böhlke, J. K. (2001). A bacterial method for the nitrogen isotopic analysis of nitrate in seawater and freshwater. *Anal. Chem.* 73, 4145–4153. doi: 10.1021/ac010088e

Sigman, D. M., Granger, J., DiFiore, P. J., Lehmann, M. M., Ho, R., Cane, G., and Geen, A., van (2005). Coupled nitrogen and oxygen isotope measurements of nitrate along the eastern North Pacific margin. *Glob. Biogeochem. Cycles* 19. doi: 10.1029/2005GB002458

Silver, B. J., Raymond, R., Sigman, D. M., Prokopeko, M., Sherwood Lollar, B., Lacrampe-Couloume, G., et al. (2012). The origin of NO3– and N2 in deep subsurface fracture water of South Africa. *Chem. Geol.* 294–295, 51–62. doi: 10.1016/j.chemgeo.2011.11.017

Silver, W. L., Herman, D. J., and Firestone, M. K. (2001). Dissimilatory nitrate reduction to ammonium in upland tropical forest soils. *Ecology* 82, 2410–2416. doi: 10.1890/0012-9658(2001)0822410:DNRTAI2.0.CO;2

Smirnov, A., Hausner, D., Laffers, R., Strongin, D. R., and Schoonen, M. A. (2008). Abiotic ammonium formation in the presence of Ni-Fe metals and alloys and its implications for the Hadean nitrogen cycle. *Geochem. Trans.* 9, 5. doi: 10.1186/1467-4866-9-5

Stanger, G. (1986). *The hydrogeology of the Oman Mountains*. (Ph.D.). Alexandria, Virginia: Open University.

Stern, J. C., Sutter, B., Jackson, W. A., Navarro-González, R., McKay, C. P., Ming, D. W., et al. (2017). The nitrate/(per)chlorate relationship on Mars. *Geophys. Res. Lett*. 44, 2643–2651. doi: 10.1002/2016GL072199

Swanner, E. D., and Templeton, A. S. (2011). Potential for nitrogen fixation and nitrification in the granite-hosted subsurface at henderson mine, CO. *Front. Microbiol*. 2, 254. doi: 10.3389/fmicb.2011.00254

Templeton, A.S. and Caro, T. (in press). The rock hosted biosphere. *Annu. Rev. Earth Planet. Sci*. doi: 10.1146/annurev-earth-031920-081957

Templeton, A. S., Ellison, E. T., Glombitza, C., Morono, Y., Rempfert, K. R., Hoehler, T., et al. (2021). Accessing the subsurface biosphere within rocks undergoing active low-temperature serpentinization in the Samail ophiolite (Oman Drilling Project). *Jour of Geophy Rese: Solid Earth*. 126, e2021JG006315. doi: 10.1029/2021JG006315

Teske, A., Alm, E., Regan, J. M., Toze, S., Rittmann, B. E., and Stahl, D. A. (1994). Evolutionary relationships among ammonia- and nitrite-oxidizing bacteria. *J. Bacteriol*. 176, 6623–6630. doi: 10.1128/jb.176.21.6623-6630.1994

Thiemens, M. H. (1999). Mass-independent isotope effects in planetary atmospheres and the early solar system. *Science* 283, 341–345. doi: 10.1126/science.283.5400.341

Thiemens, M. H. (2006). History and applications of mass-independent isotope effects. *Annu. Rev. Earth Planet. Sci*. 34, 217–262. doi: 10.1146/annurev.earth.34.031405.125026

Thiemens, M. H., and Heidenreich, J. E. (1983). The mass-independent fractionation of oxygen: a novel isotope effect and its possible cosmochemical implications. *Science* 219, 1073–1075. doi: 10.1126/science.219.4588.1073

Thiemens, M. H., Savarino, J., Farquhar, J., and Bao, H. (2001). Mass-independent isotopic compositions in terrestrial and extraterrestrial solids and their applications. *Acc. Chem. Res*. 34, 645–652. doi: 10.1021/ar960224f

Tu, Q., Lin, L., Cheng, L., Deng, Y., and He, Z. (2019). NCycDB: a curated integrative database for fast and accurate metagenomic profiling of nitrogen cycling genes. *Bioinforma. Oxf. Engl*. 35, 1040–1048. doi: 10.1093/bioinformatics/bty,741

U. S. Environmental Protection Agency (1983). "Nitrogen, ammonia. Method 350.1 (colorimetric, automated phenate)", in *Methods for Chemical Analysis of Water and Wastes EPA-600/4–79–020*. Ohio, USA: USEPA. p. 350–1.1-250–1.4.

van Kessel, M. A. H. J., Speth, D. R., Albertsen, M., Nielsen, P. H., Op den Camp, H. J. M., Kartal, B., et al. (2015). Complete nitrification by a single microorganism. *Nature* 528, 555–559. doi: 10.1038/nature16459

Verhamme, D. T., Prosser, J. I., and Nicol, G. W. (2011). Ammonia concentration determines differential growth of ammonia-oxidising archaea and bacteria in soil microcosms. *ISME J*. 5, 1067–1071. doi: 10.1038/ismej.2010.191

Verstraete, W., and Focht, D. D. (1977). "Biochemical Ecology of Nitrification and Denitrification", in *Advances in Microbial Ecology, Advances in Microbial Ecology,* Alexander, M. (Ed.). Boston, MA: Springer US. p. 135–214. doi: 10.1007/978-1-4615-8219-9_4

Vogel, J. C., Talma, A. S., and Heaton, T. H. E. (1981). Gaseous nitrogen as evidence for denitrification in groundwater. *J. Hydrol*. 50, 191–200. doi: 10.1016/0022-1694(81)90069-X

Wang, S., Pi, Y., Song, Y., Jiang, Y., Zhou, L., Liu, W., et al. (2020). Hotspot of dissimilatory nitrate reduction to ammonium (DNRA) process in freshwater sediments of riparian zones. *Water Res*. 173, 115539. doi: 10.1016/j.watres.2020.115539

Wang, X. T., Sigman, D. M., Cohen, A. L., Sinclair, D. J., Sherrell, R. M., Weigand, M. A., et al. (2015). Isotopic composition of skeleton-bound organic nitrogen in reef-building symbiotic corals: A new method and proxy evaluation at Bermuda. *Geochim. Cosmochim. Acta* 148, 179–190. doi: 10.1016/j.gca.2014.09.017

Wankel, S. D., Ziebis, W., Buchwald, C., Charoenpong, C., de Beer, D., Dentinger, J., et al. (2017). Evidence for fungal and chemodenitrification based N 2 O flux from nitrogen impacted coastal sediments. *Nat. Commun*. 8, 15595. doi: 10.1038/ncomms15595

Weigand, M. A., Foriel, J., Barnett, B., Oleynik, S., and Sigman, D. M. (2016). Updates to instrumentation and protocols for isotopic analysis of nitrate by the denitrifier method. *Rapid Commun. Mass Spectrom*. 30, 1365–1383. doi: 10.1002/rcm.7570

Welsh, D., Castadelli, G., Bartoli, M., Poli, D., Careri, M., de Wit, R., et al. (2001). Denitrification in an intertidal seagrass meadow, a comparison of 15N-isotope and acetylene-block techniques: dissimilatory nitrate reduction to ammonia as a source of N2O? *Mar. Biol*. 139, 1029–1036. doi: 10.1007/s002270100672

Weyhenmeyer, C. E., Burns, S. J., Waber, H. N., Macumber, P. G., and Matter, A. (2002). Isotope study of moisture sources, recharge areas, and groundwater flow paths within the eastern Batinah coastal plain, Sultanate of Oman. *Water Resour. Res*. 38, 2–22. doi: 10.1029/2000WR000149

Xue, D., Botte, J., De Baets, B., Accoe, F., Nestler, A., Taylor, P., et al. (2009). Present limitations and future prospects of stable isotope methods for nitrate source identification in surface- and groundwater. *Water Res*. 43, 1159–1170. doi: 10.1016/j.watres.2008.12.048

Yang, S., and Gruber, N. (2016). The anthropogenic perturbation of the marine nitrogen cycle by atmospheric deposition: nitrogen cycle feedbacks and the 15N Haber-Bosch effect. *Glob. Biogeochem. Cycles*. 30, 1418–1440. doi: 10.1002/2016GB005421

Yi, Q., Chen, Q., Hu, L., and Shi, W. (2017). Tracking nitrogen sources, transformation, and transport at a basin scale with complex plain river networks. *Environ. Sci. Technol*. 51, 5396–5403. doi: 10.1021/acs.est.6b06278

Yokochi, R., Marty, B., Chazot, G., and Burnard, P. (2009). Nitrogen in peridotite xenoliths: Lithophile behavior and magmatic isotope fractionation. *Geochim. Cosmochim. Acta* 73, 4843–4861. doi: 10.1016/j.gca.2009.05.054

Yoon, S., Cruz-García, C., Sanford, R., Ritalahti, K. M., and Löffler, F. E. (2015). Denitrification versus respiratory ammonification: environmental controls of two competing dissimilatory NO 3 – /NO 2 – reduction pathways in Shewanella loihica strain PV-4. *ISME J*. 9, 1093–1104. doi: 10.1038/ismej.2014.201

Yoshida, N. (1988). 15 N-depleted N 2 O as a product of nitrification. *Nature* 335, 528–529. doi: 10.1038/335528a0

Zhang, J., Lan, T., Müller, C., and Cai, Z. (2015). Dissimilatory nitrate reduction to ammonium (DNRA) plays an important role in soil nitrogen conservation in neutral and alkaline but not acidic rice soil. *J. Soils Sediments* 15, 523–531. doi: 10.1007/s11368-014-1037-7

Zhang, X., Sigman, D. M., Morel, F. M. M., and Kraepiel, A. M. L. (2014). Nitrogen isotope fractionation by alternative nitrogenases and past ocean anoxia. *Proc. Natl. Acad. Sci*. 111, 4782–4787. doi: 10.1073/pnas.1402976111